Loess in southwestern Sweden

Determining the genesis of the silt-rich layer rödfemman in Svartedalen nature reserve

Fanny Ekström
Anna Hedeving

Degree of Master of Science (120 credits)
with a major in Earth Sciences
45 hec

Department of Earth Sciences
University of Gothenburg
2021 B1160

Faculty of Science

UNIVERSITY OF GOTHENBURG

UNIVERSITY OF GOTHENBURG
Department of Earth Sciences
Geovetarcentrum/Earth Science Centre

Loess in southwestern Sweden

Determining the genesis of the silt-rich layer rödfemman in Svartedalen nature reserve

Fanny Ekström
Anna Hedeving

ISSN 1400-3821

B1160
Master of Science (120 credits) thesis
Göteborg 2021

Mailing address
Geovetarcentrum
S 405 30 Göteborg

Address
Geovetarcentrum
Guldhedsgatan 5A

Telephone
031-786 19 56

Geovetarcentrum
Göteborg University
S-405 30 Göteborg
SWEDEN

Abstract

The presence of loess in Sweden is relatively unexplored and has only been found in a few places. Loess acts as a paleoclimatic proxy, which in times of changing climates, is highly relevant. In 1992, Svensson wrote a master thesis on a thin and patchy silt-rich soil layer found in Svartedalen nature reserve in southwestern Sweden, in which it was proposed that the layer has an aeolian origin. In this master thesis, the sample area of Svensson was revisited and expanded. The aim was to determine the layer's genesis, age of deposition, and potential source as well as paleo-wind directions. Grain-size analysis showed a clear modality in the coarse silt region, though many samples had bimodal distributions. The findings fit well with other studies in analogous settings, where the bimodality has been interpreted as a result of mixing from either syn- or postdepositional processes. The layer is interpreted as loess due to its high silt content, Svartedalen's location above the highest shoreline, together with the layer's position in the stratigraphic record and the prevailing erosion from the last glaciation. Svensson (1992) proposed the nearby Hålt delta as the source for the silt which could not be supported in this thesis. Instead it is suggested that the silt has multiple sources in the shape of glaciofluvial deposits, sequentially activated with the retreating ice margin, or directly from the ice itself. The loess has been mixed during deposition or reworked after, shown by the grain-size distribution. OSL ages showed burial ages between 1.08 - 6.8 ka. This either reflects the date of deposition or bleaching due to reworking. An older date of 11.2 ka was derived when one sample was remeasured as this thesis was being written. A maximum age model was applied and the new date implies that the sediment has been reworked after deposition.

Key words: Loess, silt, grain-size distribution, bimodal, Optically Stimulated Luminescence (OSL), p-XRF, spatial distribution, paleowind.

Acknowledgements

In March 2020, we approached Mark D. Johnson on the hunt for a master thesis topic. When presenting different ideas, he retrieved a typewriter-printed master thesis from 1992, which he had dug up from the archives. Impressed with how well-written it was, Mark wanted to revisit the topic and bring the significance of it to light - loess found in Sweden! Mark's excitement was (as often is the case) contagious. Thus began the journey which would come to include eight field days, countless hours in the lab and an emergency visit to Uppsala. Fast-forward to a year later and here we are with our finished thesis.

We would like to thank Mark for his unwavering support and enthusiasm, without which we might not have made it through. Thank you to Thomas Zack for being our examiner, as well as helping us with developing a methodology for performing the geochemical analyses. Fredrik Andersson and Tobias Möhl who agreed to be our opponents - thanks guys! Thank you also to Britta Svensson, our predecessor, for writing a great thesis and then agreeing to meet with us to talk about it 28 years later. To Helena Alexanderson and Thomas Stevens, we would like to express our gratitude for providing essential expertise in the field of aeolian deposits and helping us out with analyses. Thomas and Vanda Jakabová rescued us when they allowed us to travel to Uppsala mid-pandemic to use the Mastersizer. Thanks also to D. Grimley and R. Schaetzl, who provided many useful pointers when dealing with loess.

We would also like to express our appreciation for the helpful teachers and students of GVC. Thank you to Louise Andresen, Matthias Konrad-Schmolke, Tobias Rütting and Delia Rösel, your expertise and feedback was much appreciated. Izabella Remmert and Jakob Isaksson, thank you for your help in the lab.

Finally, thanks to our partners, families and friends. Without you, none of this would have been possible.

The Loess Ladies - Fanny and Anna

Contents

List of Figures

List of Tables

1 Introduction

Loess is a windblown sediment that occurs globally. It is highly researched as loess can serve as a proxy for paleoclimate (Marković et al., 2008; Stevens et al., 2011), and atmospheric dust can force the climate by complex feedback loops (Miller et al., 2014). Furthermore, dust also has an impact on ecosystems as it can increase bio-productivity by contributing nutrients (Okin et al., 2004; Mahowald et al., 2005). Its paleoclimatic information makes loess research of high interest in a time of changing climates. The most famous and thoroughly studied loess deposit is the great Chinese loess plateau, which shows a catalogue of many repeated times of loess deposition alternated by soil formation. These alternating layers are linked to glacial and interglacial periods, thus presenting a useful paleoclimatic record (Yang in Schaetzl et al. (2018)).

In Sweden loess has rarely been described. There are three localities where sediment interpreted as loess have been found and scientifically investigated: Brattforsheden in Värmland, Svalsjö in Småland, and Mora in Dalarna (Agrell & Hultman, 1971; Fredén, 2001; Hjulström et al., 1955). However, Björsjö (1949) mentions a layer referred to as *rödfemman* or *fimman*. *Rödfemma* is a surface silt-rich layer that has a characteristic red colour due to its occurrence in the B-horizon in the soil. This layer has been mentioned before as being silt deposited by wind (Hillefors, 1969). Svensson (1992) also mapped *rödfemma* in Svartedalen in southwestern Sweden. Based on her analysis, principally of grain size, it was interpreted as loess.

1.1 Aim of study

This thesis aims to investigate the genesis of the silt-rich layer known as *rödfemma* in Svartedalen. This entails collecting and analysing samples for grain-size distribution, geochemistry and Optically Stimulated Luminescence (OSL) derived ages. We wish to determine what depositional and post-depositional geological process has resulted in this

unique layer of sediment as well as determine its provenance.

1.2 Hypothesis

Based on the results from Svensson (1992), it is expected that the genesis of the silt-rich layer is aeolian and that the silt can be sourced to glaciofluvial deposits. Further, it is believed that a fining trend in grain size from the northwest to southeast will be seen as the silt has been deflated by katabatic winds from the ice sheet. As the wind's carrying capacity is limited, it is hypothesised that the smaller grain-size fractions has a higher ratio of heavy minerals than the larger fractions. This would entail at a certain distance from the source, high-density minerals will be smaller than low-density minerals. It is further hypothesized that deposition occurred closely after the retreat of the ice as there at this point would not have been any vegetation to prevent deflation. Additionally, the layer could not have been deposited prior to the ice-sheet retreat due to the glacier's highly erosive forces.

1.3 Study area

The area of interest is located in the nature reserve Svartedalen north of Gothenburg (Figure 1.1). Svartedalen is located in the so called Idefjorden terrane, and bedrock mostly consists of different granites and gneisses (Figure 1.2). It is a joint-valley landscape with exposed bedrock (Figure 1.2) and sometimes with a thin layer of unconsolidated sediment on top. In the valleys, clay has been deposited and peat is also abundant (Figure 1.3). The study area is mainly above the highest shoreline. In the surficial geology map, a number of glaciofluvial deposits can be seen, one of them being the Hålt delta (Figure 1.3) in the northeastern corner of the research area (Fredén, 1986).

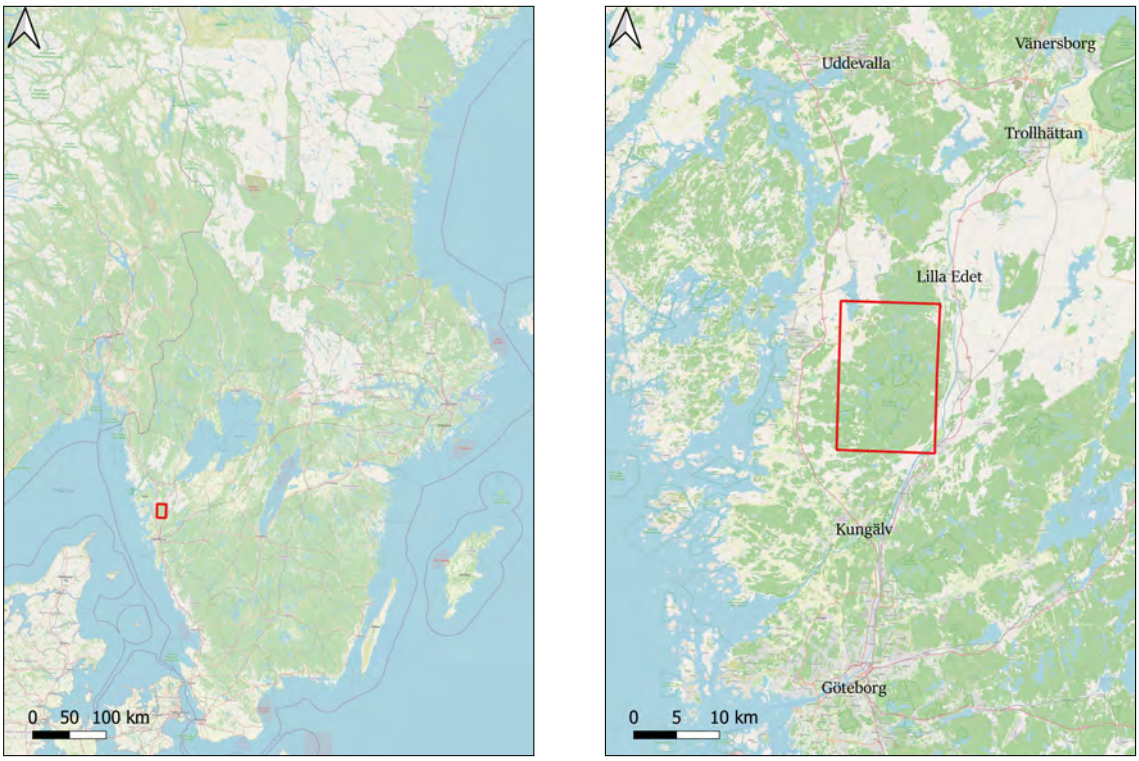

(a) **(b)**

Figure 1.1: An overview of the study site marked with a red box in the maps. Data: © OpenStreetMap contributors, CC-BY-SA

1.3.1 Geological background

The bedrock in the area is referred to as the Idefjorden Terrane and was mainly created during two different orogenies, the Gothic and the Sweconorwegian (Lundqvist, 1997). During the Gothic orogeny (1.75 - 1.55 Ga), intrusive and extrusive rocks as well as rocks with sedimentary origin were created (Lundqvist, 1997). There was extensive deformation and transformation of the rock in amphibolite facies, and great amounts of differentiated calc-alakaline magmas intruded (Lundqvist, 1997). The study area is located in the Idefjorden Terrane that consists of grantoids and gneisses (Petersson et al., 2015). After the intraorogeny, an intracontinental

bimodal magmatism occurred (Lundqvist, 1997). During the Sveconorwegian orogeny, the rocks were subjected to metamorphism (1.15-0.90 Ga) (Lundqvist, 1997). The eastern edge of the Idefjorden Terrane is marked by the Mylonite Zone (Sturkell & Hegardt, 2020).

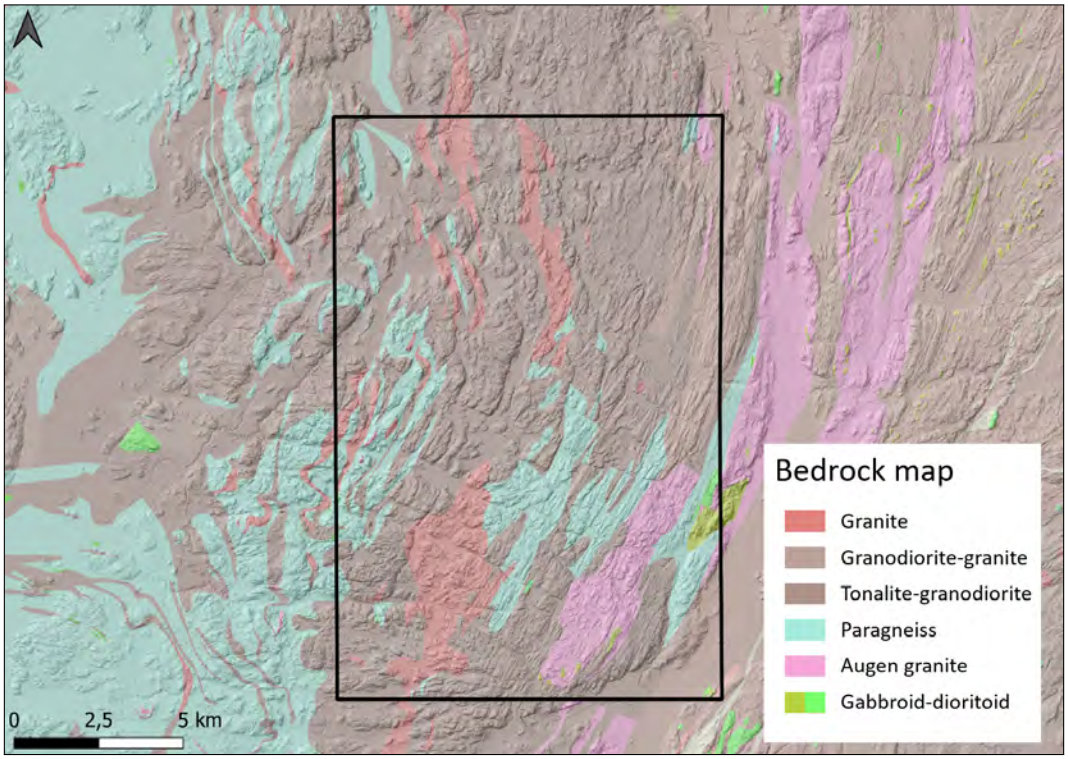

Figure 1.2: A geologic map of the bedrock. © Lantmäteriet Höjdmodell. Data: © SGU Geologisk enhet, yta

Post-orogenic instrusions in form of granites, pegmatites and diabase occurred after the Sveconorwegian orogeny (Lundqvist, 1997). Marine sediment was deposited during the Cambrium, which formed sedimentary rocks. These were intruded by a diabase during Permian which protected the easily eroded sedimentary rocks, creating the Västgötabergen (Lundqvist, 1997). In southwestern Sweden following orogenesis, a long period of quiet allowed the erosion of the mountains that had been produced and eventually the formation of a peneplain (Lidmar-Bergström, 1996). The peneplain was created during the late Proterozoic to early Paleozoic, and during Mesozoic deep rock weathering created an etched

surface, forming joint valley landscapes and undulating surfaces (Lidmar-Bergström, 1995).

1.3.1.1 Quaternary development

Sweden has been glaciated several times during the Quaternary. The Weichselian glaciation was the most recent (Svendsen, 2004) during which Sweden was covered by the Fennoscandian ice sheet, with its maximum extent between 26.5 to 20 ka (Clark et al., 2009). Deglaciation occurred between 22 cal ka BP to 9.7 cal ka BP (Stroeven et al., 2016). The ice sheet had its origin in the Scandinavian mountains (Ehlers & Gibbard, 2004) and reached its maximum extent during the late Weichselian. At this time the ice sheet had connected to others and together they covered an area between Ireland and the Taymir Peninsula (Svendsen, 2004). As the ice margin began to retreat, several moraines formed (Stroeven et al., 2016). Svartedalen is located between the Gothenburg moraine and Berghem moraine. This means that the deglaciation of the area Svartedalen occurred between 14.7 and 14.0 cal kyr BP (Stroeven et al., 2016). The Hålt delta, which lays in the northeastern part of the study area, was interpreted as an ice-marginal deposit by Björsjö (1949) and included as a portion of the 'Berghem Moraine' by Johansson (1982) and Stroeven et al. (2016). In addition to the delta, a subtle end moraine can be traced for several kilometers to the northwest from the Hålt delta. During the deglaciation of Fennoscandia, a shoreline displacement occurred due to isostatic rebound and eustatic sea level change (Fjeldskaar, 1991; Mörner, 1969, 1971, 1972; Påsse, 1996; Påsse & Andersson, 2005). The highest shoreline (or marine limit) represents the maximum extent of the sea after deglaciation. There are several geomorphological features that reveals the location of the highest shoreline. In Svartedalen the Hålt delta is a such a feature and here the highest shoreline is 120 m.a.s.l.

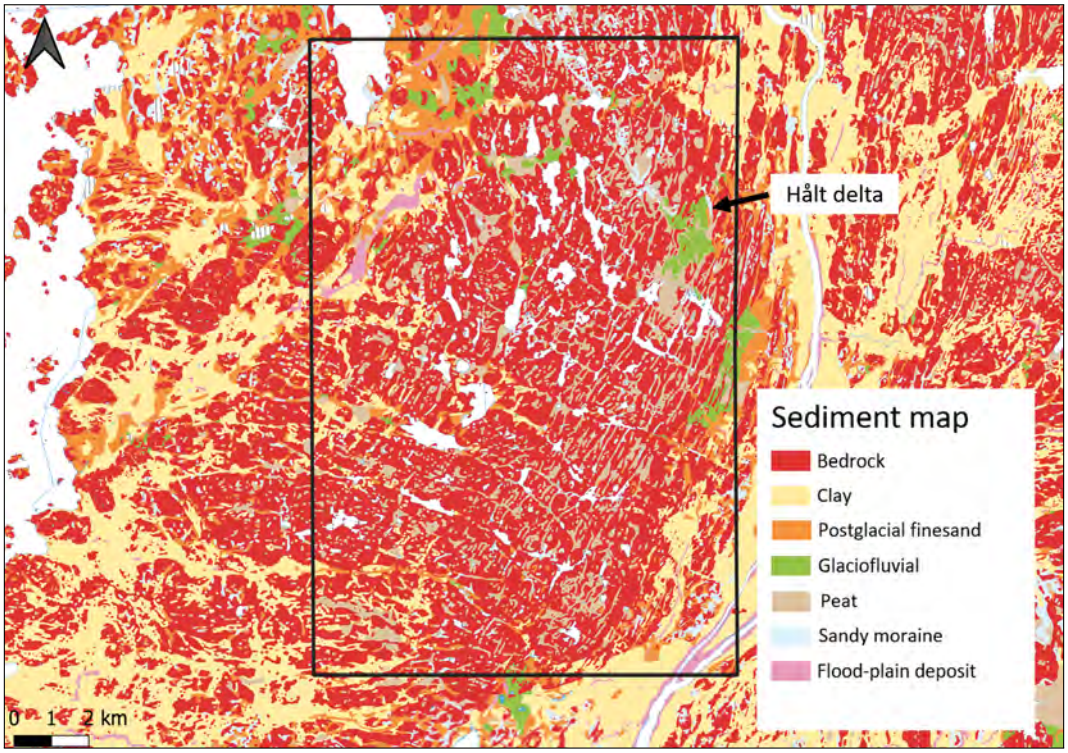

Figure 1.3: A geologic map showing surficial geology. Data: © SGU Jordart, grundlager

Svartedalen is largely elevated above the highest shoreline. East, south and northwest of Svartedalen several glaciofluvial deposits are located. In areas below the highest shoreline fine sediments, such as clay, are present (Fredén, 1987, 1986)

1.4 Loess

The definition of loess has been a source of debate and even the subject of several articles (Pécsi, 1990; Smalley et al., 2011; Sprafke & Obreht, 2016). Opinions differ as to whether only grain-size distribution and aeolian origin should be taken into account, or if certain criteria also must be met in regards to cementation and mineral content (Pécsi, 1990). This thesis will use the definition proposed by (Muhs et al., 2014); loess is a sediment dominated of particles in the silt fraction that have been deposited by wind. Both Pécsi (1990) and Muhs et al. (2014)

note that loess is generally well sorted. Pécsi (1990) writes that 50-70% is in the range of 10-50 microns, whilst Muhs et al. (2014) says 60-90% is in the range of 2-50 microns.

Loess is formed when strong winds deflate silt-rich sources and deposits the dust in a different location as its carrying capacity wanes. Muhs & Bettis (2003) note that sources are usually associated with glacial activity as the erosive powers of the ice produce large quantities of silt which then accumulates in outwash deposits, from which silt can be easily deflated. However, they also describe other processes that can generate sufficient amounts of silt, such as wind abrasion and fluvial comminution.

1.4.1 Loess in Sweden

Loess in Sweden is relatively sparse and thin and has only been interpreted to occur in three locations; Brattforsheden, Mora field and Svalsjö field, (Agrell & Hultman, 1971; Fredén, 2001; Hjulström et al., 1955). However, it is implicitly mentioned in soil map descriptions from SGU (Swedish Geological Survey) in a few more places (Magnusson & Lundegårdh, 1972; Fredén, 1997). Due to the highly erosive forces of the latest glaciation of Fennoscandia, loess deposits in Sweden are not expected to be thick. They will not show the cyclical paleosoil data which can be seen in the Chinese Loess Plateau. Loess found in Sweden should thus have been deposited after the final ice-sheet retreat from the area. Loess south of the dune field in Brattforsheden is the best studied in Sweden (Enquist, 1932; Hjulström et al., 1955; Hörner, 1927) with a thickness ranging between a few decimeters to a meter. Enquist (1932); Hjulström et al. (1955); Hörner (1927) argued the windblown silt was deposited by anticyclonic winds from the retreating ice sheet. In Northern America, thin loess deposits like the one in Brattforsheden and Svartedalen also exist and these have been argued to have been deposited by katabatic winds originating from the ice sheet (Schaetzl & Attig, 2013).

Svensson (1992) interpreted that the silt-rich layer in Svartedalen to be of aeolian origin. Samples were taken from ten locations in a NNE-SSW line, and a trend of fining grain sizes away from the northern Hålt delta was shown. Svensson concluded that this delta was the likely source.

2 Method

2.1 Field work

Field work was conducted in June and October of 2020. Locations from Svensson (1992) were revisited to collect samples of the surface silty sediments as well as an additional 18 new locations. A total of 92 samples were collected. The new locations were determined using the highest shoreline as a delimiting factor, all areas below the highest shoreline were avoided (Figure 2.1).

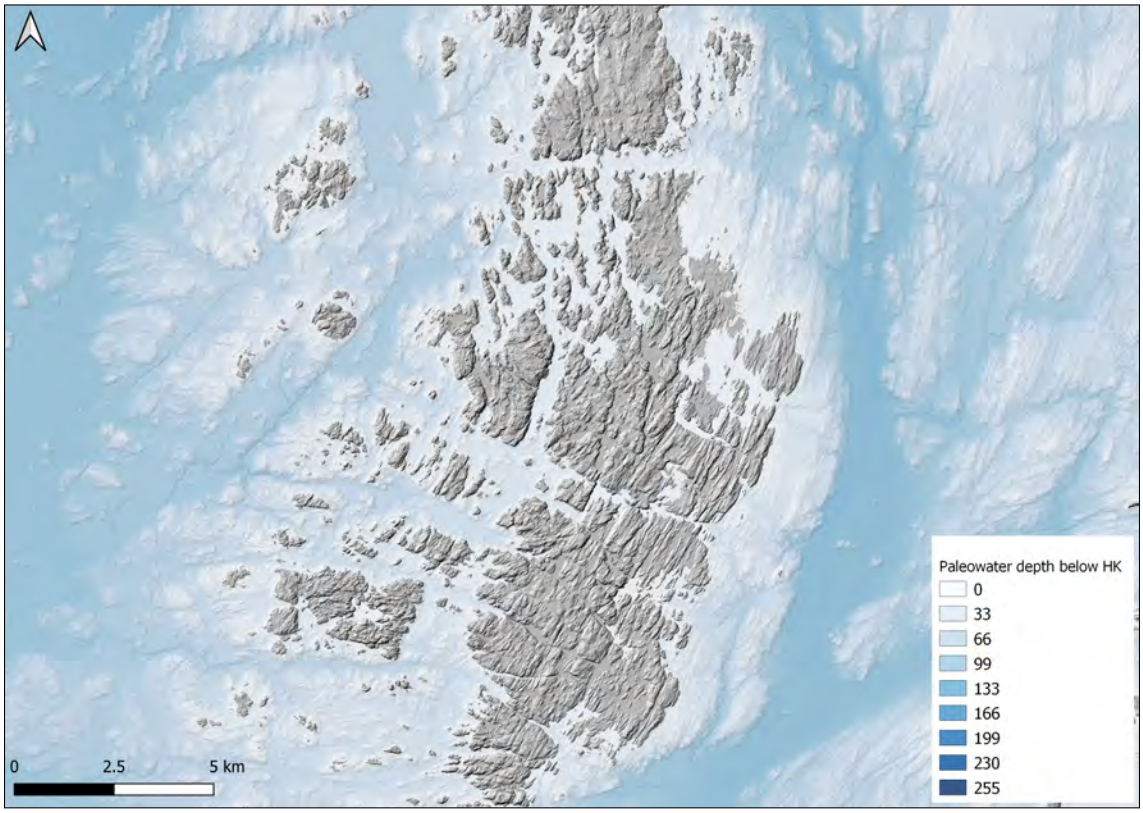

Figure 2.1: Svartedalen topography outlined by the highest shoreline and the water depth at the time. Data: © Lantmäteriet Höjdmodell, © SGU Highest shoreline

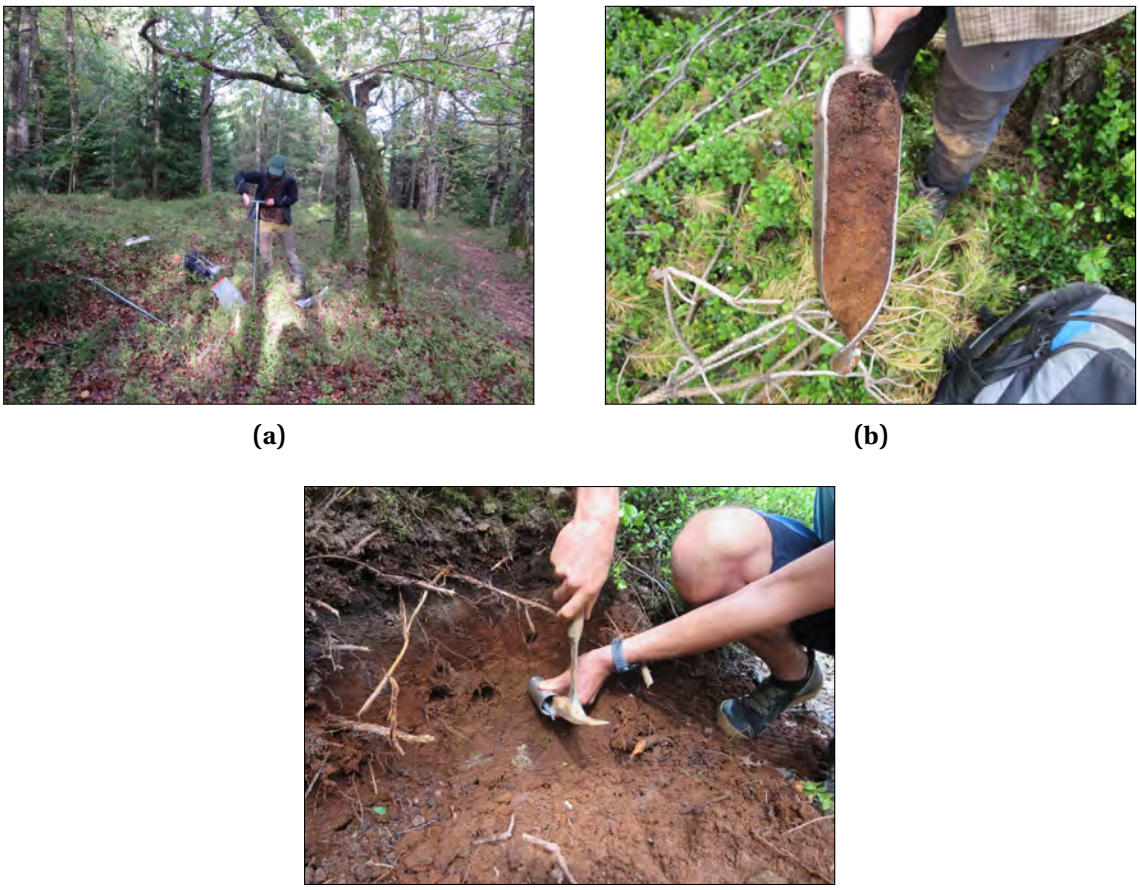

(a) **(b)**

(c)

Figure 2.2: Pictures from field work showing various aspects (a) sampling (b) a picture of the auger with the silt rich sediment and (c) OSL-sampling with tube.

At each location, at least one sample was taken using a handheld auger (see Figure 2.2) and the soil thickness was determined. In some localities, a coarser sediment was below the silt-rich layer and samples of this were taken as well. At many locations, however, the silt-rich layer was thin and avoiding the inclusion of some underlying coarser sediment was not possible. Because of the thickness of the silt layer, all localities shown have been affected by soil development. All samples collected ended up being within the B horizon. At each sampling site, thorough notes were taken on the location's surroundings, topographic

conditions, silt colour and thickness as well as a description of the stratigraphy. Three locations provided sufficiently thick layers for a profile to be sampled at a 5cm interval.

At seven locations, OSL-samples were taken. Six samples were taken using a handheld auger and black plastic bags, and one using a metal tube. Out of these, five were sent to Lund University for dating. As it is important that the samples are collected in total darkness, double black plastic bags were used to shield the samples from light. The handheld auger was placed in a small hole at the bottom of the bags while the bag openings were securely held against the ground, limiting light. A first auger sample was taken vertically and dumped in order to remove the upper organic layer. A new auger sample was taken from the soil below the first, this one being emptied within the plastic bags and quickly sealed. The samples were finally duct taped shut to properly shield it from any light that might cause bleaching. The sample taken using the metal tube was clubbed in horizontally to a sediment profile with the outer end blocked from sunlight using duct tape. Once inserted fully, the now filled tub was dug out and sealed at the other end (Figure 2.2c). The OSL samples were analyzed by Professor Helena Alexanderson in the Lund Luminescence Laboratory.

2.2 Lab work

Lab work took place from October 2020 to January 2021 in two different stages with the first stage being grain-size analysis in Uppsala and the second stage p-XRF analysis.

2.2.1 Grain-size analysis

The determination of grain-size distribution was conducted by dry sieving and using a Malvern Mastersizer® at Uppsala University (Figure 2.3). For each sample, an approximate half teaspoon was measured after passing a 2mm dry sieve and placed in a beaker. H_2O_2 , [33%], was then added to a level of 2cm above the soil in order to dissolve organic material. After the reaction had ceased, the sample was washed three times by decanting the liquid

and refilling with distilled water. In order to avoid decanting unsettled finer particles, cloudy samples were heated in a water bath instead of being poured out. The samples were kept in suspension and kept from drying as to avoid flocculation. After washing, samples were transported to Uppsala suspended in distilled water in sampling tubes.

The samples were analysed in Uppsala by a Malvern Mastersizer X in December 2020. It uses laser diffraction to measure the amount of sediment in particular grain-size classes. By using theories about how particles scatter light, the Mastersizer can determine the size of the particles (Malvern, 1997). The scattering pattern is picked up in the optical unit that consists of several detectors. The optical unit takes about 2000 sweeps each run. After this the measurements can be analysed in the Malvern software (Malvern, 1997).

Figure 2.3: Mastersizer X

Before the samples were run through the Mastersizer X, a dispersing agent was added, in the form of $Na_4P_2O_7$. The samples were then put in an ultrasonic bath to disperse further. Each sample was agitated and then a small amount was added to the Mastersizer X using the settings shown in Table 2.1 until obscuration reached levels between 12 and 20%. Each

sample was run at least three times. The Mastersizer X was rinsed with distilled water between samples until the background was reduced to normal values.

Table 2.1: Standard settings used for the grain-size analysis with the Malvern Mastersizer X

Property	Setting
Density	2.65 g/cm^3
Lens thickness	300mm
Unit	MSX1
RI	Glass
Histogram width	Standard

The Mastersizer produced data consisting of mass percentages from grain sizes starting at a couple of microns. Modes from each sample run was also produced. The mass percentage data was then compiled cumulatively from coarse to fines and converted to the phi-scale. From this the grain size for specified percentiles was noted and used in calculating the sorting (σ_1), skewness (Sk) and kurtosis (K) according to the formulas from Folk & Ward (1957) shown below (Equation 2.1, 2.2, 2.3). Folk and Ward values to be used for categorising these parameters and the samples were classified accordingly (See Table 2.2, 2.3, 2.4).

$$\sigma_1 \ \frac{\phi 84 - \phi 16}{4} \ \frac{\phi 95 - \phi 5}{6.6} \tag{2.1}$$

$$Sk \ \frac{\phi 16 \ \phi 84 - 2\phi 50}{2(\phi 84 - \phi 16)} \tag{2.2}$$

$$K \ \frac{\phi 95 - \phi 5}{2.44(\phi 75 - \phi 25)} \tag{2.3}$$

Table 2.2: Sorting (Folk & Ward, 1957; Prothero, 2014)

Calculated value	Classification
≤ 0.35	Very well sorted
0.35-0.50	Well sorted
0.50-1.00	Moderately sorted
1.00-2.00	Poorly sorted
2.00-4.00	Very poorly sorted
≥ 4.00	Extremely poorly sorted

Table 2.3: Skewness (Folk & Ward, 1957; Prothero, 2014)

Calculated Value	Classification
-1.00 - -0.30	Very coarse-skewed
-0.30 - -0.10	Coarse-skewed
-0.10 - +0.10	Unskewed
+0.10 - +0.30	Fine-skewed
+0.30 - +1.00	Very fine-skewed

Table 2.4: Kurtosis (Folk & Ward, 1957)

Calculated value	Classification
≤ 0.67	Very platykurtic (very deficiently peaked)
0.67-0.90	Platykurtic (deficiently peaked)
0.90-1-11	Mesokurtic (normally distributed)
1.11-1.50	Leptokurtic (peaked)
1.50-3.00	Very leptokurtic (very peaked)
≥ 3.00	Extremely leptokurtic (extremely peaked)

With the modes derived from the Mastersizer 2000, regional maps showing variations in the grain-size statistics were made. Four maps were created using different input data criteria in order to demonstrate variations in the maps. Depending on which criteria used to delimitate the input data for the runs, different maps were created. The interpolated maps were created in ArcGIS by using Inversed Distance Weighting (IDW). Different modal values were selected to represent the grain-size distribution in four runs. What is included in the different runs can be seen in Table 2.5. The first run includes one sample from each location. Where locations had multiple sampling sites, the sample site situated on a topographic high point was selected to represent the modal grain size for that location. If there was no sample from a topographic high point, the samples located topographically highest were chosen. For the second run the input data was limited to samples with a clear silt mode. In the third and fourth bimodality

was considered. In the third run all samples were used, but when there was a bimodadlity the modal value in the silt range was selected and in the fourth only the best silt samples were picked out. Further the interpolated modes were clipped in ArcGIS with the outline of the highest shoreline to discard areas below the highest shoreline. The newly created layers were exported to Q-GIS and maps were created.

Table 2.5: Description of runs for regional maps

Run	**Description**
Run 1	One value used for every location. If multiple site within one location, site on topographic high point selected
Run 2	One value used for every location. If multiple sites within one location, the site with the clearest silt mode selected. Only primary mode used.
Run 3	All sites used and when bimodality is present silt mode chosen
Run 4	Only locations with a clear silt mode selected and for samples with bimodality, the clear silt was mode selected

2.2.2 Geochemistry

Geochemistry of the sediments was analysed with p-XRF (Portable X-Ray Fluorescence). In addition to analyzing the surface silt, two samples of till exposed at Dösebacka, located 5 km south of the field are, were also taken. The till is assumed to represent the debris transported in the ice. The elements titanium (Ti), zirconium (Zr) and silica (Si) were analysed on 10 different samples and for two different grain size intervals, 62.5-88.4µm (4-3.5Ø) and 44.2-62.5µm (4.5-4Ø) giving a total of 20 samples. To isolate the grain-sizes, both wet-sieving and dry-sieving was conducted. Organic material was removed using H_2O_2 , sieving and

settling. The sediments were washed three times afterward to ensure that all H_2O_2 was rinsed away. Wet sieving was performed in two stages. First, the sediments were sieved through a 62.5µm mesh to collect the grains larger than 62.5 microns on the mesh as well as the grains smaller than 62.5µm in a beaker beneath the sieve. The clay and silt that passed the mesh were wet-sieved again through a 44.2µm mesh, the sediments left on the sieve were collected as the 44.2-62.5µm, i.e. coarsest coarse silt, fraction. The sediment was dried in an oven at 105°C. The dried >62.5µm sediment could then be dry-sieved to isolate the 62.5-88.2µm fraction, i.e. the finest very fine sand, from here on referred to as the finest sand. For all the samples an amount of 2-3g was collected in plastic holders, 5mm thick and a diameter of 13mm and 21mm for the inner ring and outer ring respectively (see Figure 2.4b). The sediment was compacted using a weight and covered with a thin plastic film. With p-XRF (Olympus Delta Premium) the samples were analysed. The 'mining mode' was used for analysing the samples. Both the first and second beam were set to 30 seconds.

The p-XRF emits x-ray photons with high energy. When these photons hit the atoms within the sample, it creates a specific energy that can characterise the element and the intensity of that energy determines the amount of that element. This energy is created because atoms have orbitals with electrons surrounding its nucleus and when the photons emitted from the p-XRF hits the atom the innermost electron gets excited and is ejected. A vacancy is created in the inner orbital and makes the newly created ion unstable therefore an electron from the one of the outer orbital moves down to the vacant spot created. The energy emitted is a secondary x-ray photon and the phenomenon is called fluorescence (Olympus, 2015) (See Figure 2.4c).

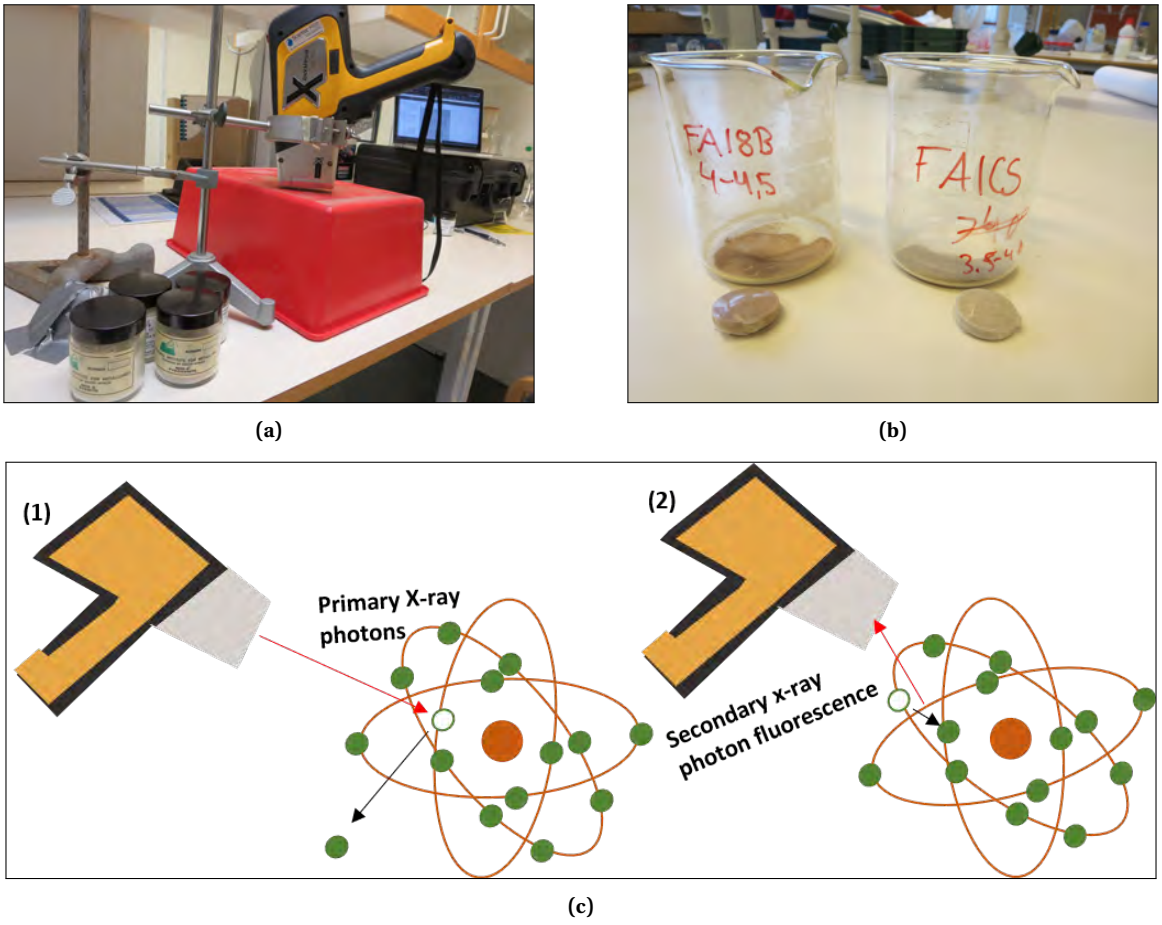

Figure 2.4: The figure displays (a) the setup using Olympus Delta p-XRF, (b) the pucks used for analysis and (c) how the p-XRF works, figure influenced by (Malvern, 1997). First (1) the p-XRF sends out primary X-ray photons that excites the innermost electron and it gets emitted. Thereafter (2) a electron from a outer shell moves to the vacant and emits a secondary X-ray photon fluorescence that the detector in the p-XRF picks up

Before analysing the samples, calibration of the method from certified reference material (CRM) was conducted. The CRM used comes from the Council for Mineral Technology Republic of South Africa. The samples used where SARM 51 (Stream Sediment), SARM 50 (Dolerite), NIM-P (Pyroxenite), NIM-S (Syenite), NIM-G (Granite), SARM 46 (Stream sediment), SARM 49 (Quartz), and SARM 52 (Stream sediment). By preparing the CRM

samples in an identical manner as the silt and sand samples, it could be assured that the sample holder, amount, and coverage was the same. With this, the margin of error could be determined. The values for Si, Ti and Zr in the silt and sand samples could be corrected with a ratio determined from the CRMs, see table 2.6.

Table 2.6: Table shows the ratios calculated from the certified reference material (CRM). Dashed columns means that the element was not present in the CRM or that due to a low value the ratios were deemed as non trust worthy.

Ratios for p-XRF			
CRM	Si	Ti	Zr
NIM-G	1.237	-	1.148
SARM 49	1.241	-	-
NIM-P	1.445	1.430	-
NIM-S	1.263	-	-
SARM 50	1.388	1.386	0.894
SARM 52	1.578	1.569	0.987
SARM 51	1.344	1.556	1.034
SARM 46	1.289	1.575	1.156
Average	1.357	1.503	1.156

The combined group of Zr and Ti was compared to Si as it has been shown that loess is relatively depleted in heavy minerals such as rutile (TiO_2), titanite ($CaTiSiO_5$), and zircon ($ZrSiO_4$) as an effect of sorting from wind transportation (Schaetzl & Loope, 2008). The surface silt from Svartedalen was compared to till from Dösebacka as the till should not be depleted in heavy minerals.

2.2.3 OSL Dating

The samples were dated using optically stimulated luminescence (OSL). When a mineral is buried it gets charged as the natural environmental radiation causes electrons to be trapped

in the crystal lattice. This charge can be measured in a laboratory (Rhodes, 2011). The trapped energy is released when subjected to light and the build-up of radiation tells the amount of time that has passed since burial. This indicates the age since the mineral last was on the surface and exposed to light (Rhodes, 2011). To determine the age of the samples, both equivalent dose, D_e, and the dose rate is needed, from which the age can be calculated (see Equation 2.4). The equivalent dose is measured in the laboratory and the dose rate is determined to calculate the age (Rhodes, 2011).

$$Age(years)\ \frac{D_e(Gy)}{\textit{Dose rate (Gy/year)}} \tag{2.4}$$

The dating of the samples was conducted in Lund Luminescence laboratory by Helena Alexanderson. Five samples were dated, two from the same location. Grains of quartz between 63µm and 90µm were separated and analysed. To be able to determine the age of the sediments, the water content and dose rate was also investigated. Between 26 and 30 aliquots were measured per sample. For more information about the methodology, see Appendix B.

3 Results

All the sample locations visited can be seen in Figure 3.1. A total of 29 locations were visited. At all sites, a surface layer of silt was identified and sampled.

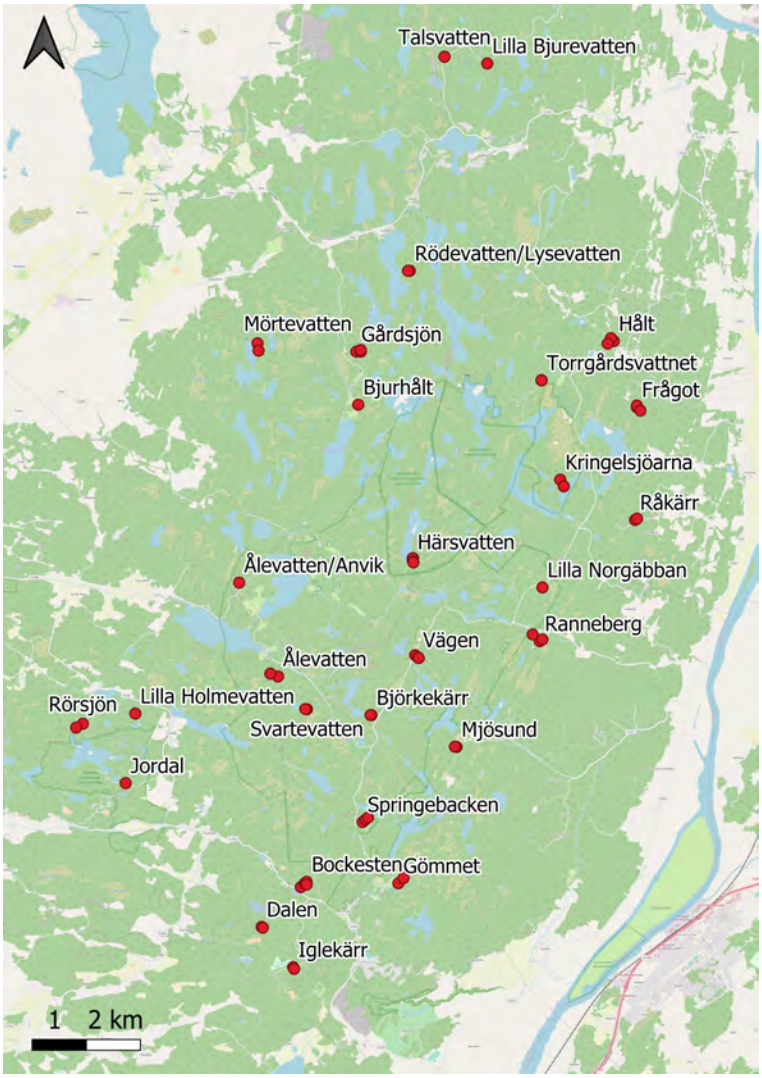

Figure 3.1: The 28 sample locations marked with red dots.© OpenStreetMap contributors, CC-BY-SA

The silt-rich layer is discontinuously distributed over Svartedalen, leading to range in its thickness locally. In some locations, the silt-rich layer could be found in topographic depressions in an area otherwise dominated by exposed bedrock. All locations had clearly developed O-, A- and B-horizons. In some of the locations, a clearly developed E-horizon could also be seen. The silt-rich layer is in places deposited on top of gravelly sand material but more often directly on top of the bedrock. The thickness of the silt-rich layers ranged from 15cm to 80cm, but most commonly varied between 20cm to 40cm. The thickness varied depending on the landscape; almost all locations that have the greatest thicknesses are all located in topographic depressions, with some exceptions.

3.1 Grain-size distribution

Samples from Svartedalen show different patterns in grain-size distribution, some are bimodal, others unimodal and some have 'shoulders'. Shoulders are a planing out pattern in the grain-size-distribution occurring either on the coarser of finer limb of the primary mode. An example of this is location Rörsjön site A in Figure 3.3f. The planing out feature creates a shoulder on either the fine side or the coarse side or a shoulder on each side. Out of 61 samples, 17 are bimodal and 44 are unimodal (see Table 3.1). Out of the 44 unimodal samples, 2 are unimodal without any shoulders, 15 have a shoulder on the fine side, two have a shoulder on the coarse side, and 25 have a shoulders on each side.

Table 3.1: The table shows the groups using the grain size distribution pattern, profiles are not included.

Group	**Number of samples**
Bimodal	17
Unimodal total	44
Unimodal without shoulder	*2*
Unimodal shoulder on fine side	*15*
Unimodal shoulder on coarse side	*2*
Shoulder on both coarse and fine side	*25*

The grain sizes range from clay to coarse sand. The modal values can be seen in Figure 3.2. The modes range from as small as 7.5Ø up to 0.5Ø (5.5-707µm) for the bimodal samples, or 5.5Ø up to 1.5Ø (23.1-353.5µm) for the unimodal values. The bimodal samples have a primary mode and a secondary mode and both are presented in Figure 3.2. Primary modes varies between 5Ø and 2Ø (31.25-250µm) and the secondary modes have a greater variation with modal values between 7.5Ø up to 0.5Ø (5.5-353.5µm). The majority of the samples' modal values are in the coarse silt fraction, 5Ø up to 4.5Ø (31.25-44.2µm), Figure 3.2.

The modes of the bimodal and unimodal samples can be seen in Figure 3.2, and examples can be seen in Figure 3.3a-b and d-f. The location Ålevatten consists of three samples from two sites where one of them, site A, has a clear bimodality and no substrate sample was collected. Site B is the other sample site at the location Ålevatten, where a substrate sample and sample of the surface silt was collected. Site A in location Ålevatten shows a clear bimodality with peaks coinciding with both the surficial silt and the substrate in the same site (site B), Figure 3.3c.

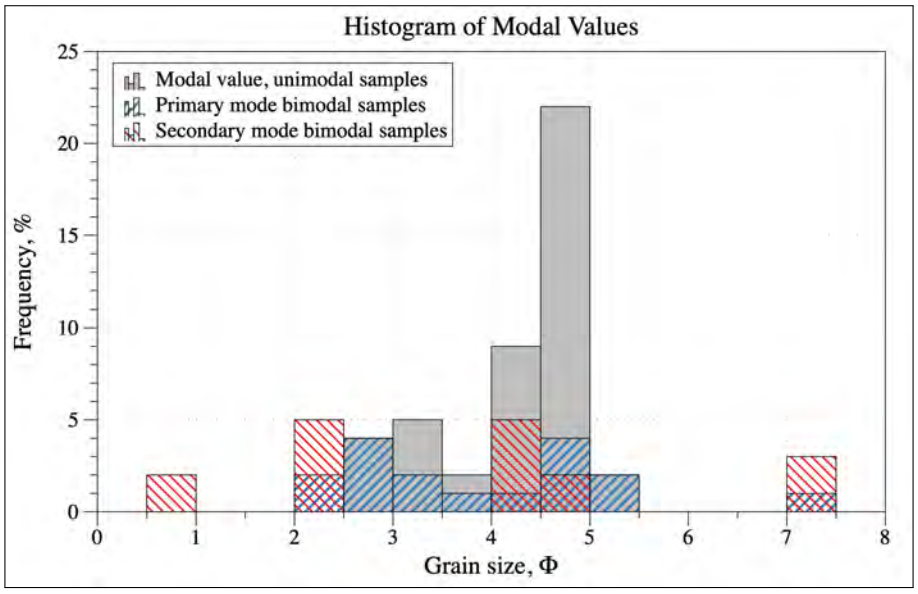

Figure 3.2: Histogram over the modal values of all the samples. The grey bars represents the samples with unimodal modes. Bimodal samples are represented by striped bars, the primary modes have samples blue stripes and the secondary modes have red stripes.

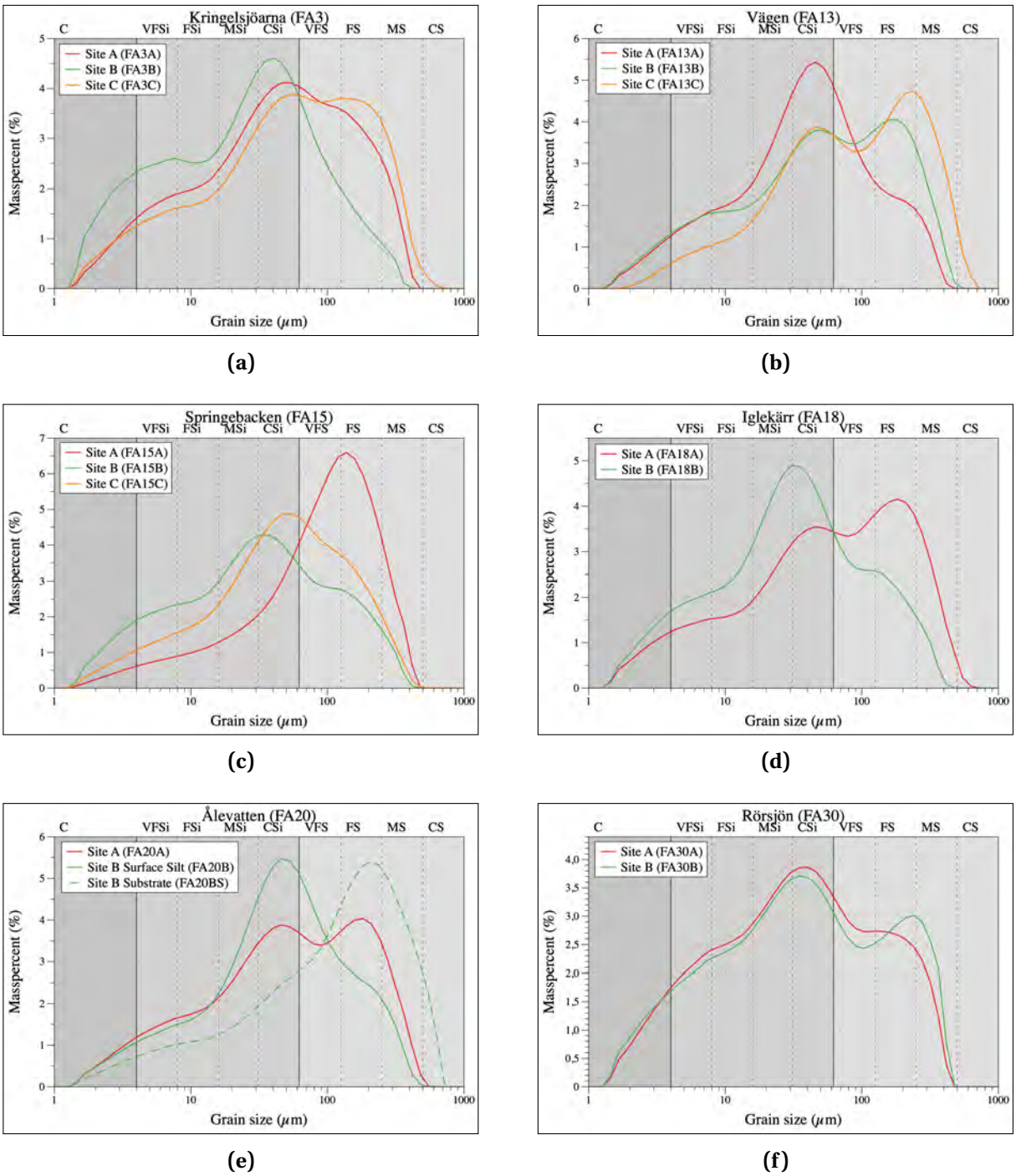

Figure 3.3: Representative grain-size distributions from six different sites are presented, each location have multiple sites where samples were collected. In the figure samples from the locations (a) Kringelsjöarna, (b) Vägen, (c) Springebacken, (d) Iglekärr, (e) Ålevatten, and (f) Rörsjön are presented. All grain-size curves are of the surface silt, except for e, which also includes a curve of the substrate sediment.

Most samples are unimodal (Table 3.1), but only two are without shoulders. The two samples with a unimodal distribution without shoulders are finely skewed and have modal values in the fine sand fraction. An example of this can be seen in Figure 3.3c.

Samples that have a shoulder on the fine side are 15 in total (Table 3.1). An example of this type of a shoulder on the fine side but in a bimodal can be sen in Figure 3.3d, site A. Only two samples have shoulder on the coarse side, an example of this is Figure 3.3c

There are also samples that have shoulders on both the coarse and fine sides on the grain size distribution. Double shoulders are present in 25 samples. This is the most common grain-size distribution, with a distinct mode and a shoulder on both the coarse and fine grain-sizes. The pattern of the shoulders inside this group can vary and the shoulder can be larger on either side of the mode. An example where the shoulders are quite similar is location Iglekärr site A in Figure 3.3d. This kind of pattern can also be seen in location Ålevatten site A in Figure 3.3c, location Vägen site A in Figure 3.3b and location Springebacken site B in Figure 3.3c. However, some samples also have different sizes of the shoulders, this can be seen in location Kringelsjöarna site A Figure 3.3a. Here the shoulder is larger on the coarse side and a smaller shoulder on the fine side, but the sample is still regarded as fine-skewed in the statistics Figure 3.5. In Figure 3.3f the shoulder of location Rörsjön site A coincides with the secondary mode of site B, the same pattern is also apparent in Figure 3.3a.

3.1.1 Grain-size statistics

Values of sorting, skewness and kurtosis are shown below in Figure 3.4, Figure 3.5 and Figure 3.6. Figure 3.4 shows that the samples are poorly to very poorly sorted. Figure 3.5 shows that a majority of the samples were either unskewed or fine-skewed. The coarser the modal grain size, the more fine-skewed the sample appears. A few samples plot in the very fine-skewed area, including 3 of the 4 substrate samples. The kurtosis of the samples are not extreme and plot as leptokurtic (peaked), mesokurtic (normally distributed) or playkurtic (deficiently peaked) without showing a trend (Figure 3.6).

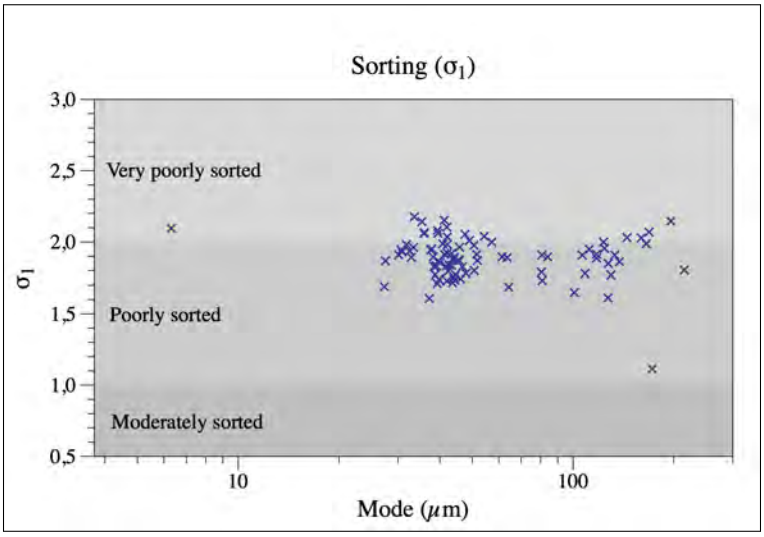

Figure 3.4: Sorting calculated for the samples analysed. Crosses are showing results for the silt rich soil layer.

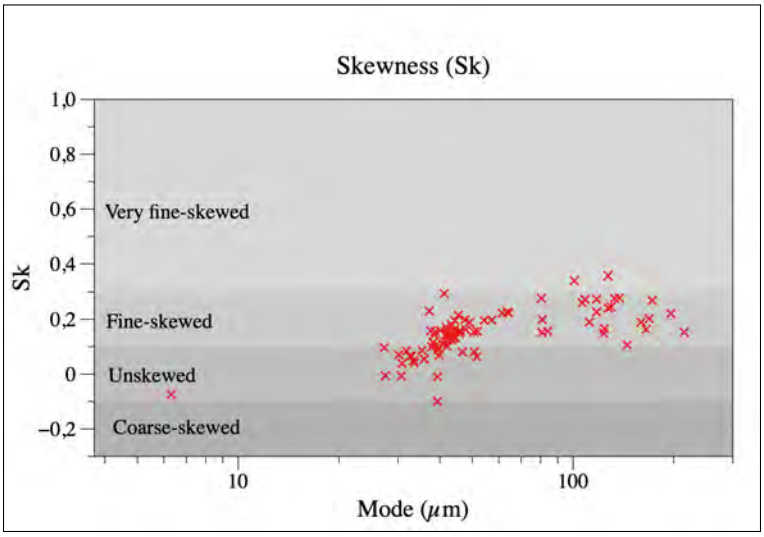

Figure 3.5: Skewness calculated for all analysed samples plotted against modal grain sizes. Crosses represent values for the silt rich soil layer.

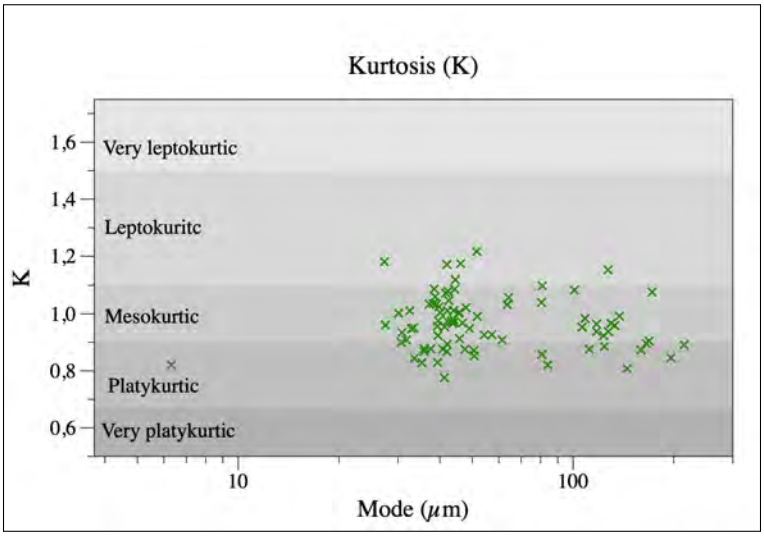

Figure 3.6: Calculated kurtosis for all analysed samples plotted against each sample's modal grain size. Plotted as crosses are samples of the silt rich soil.

3.1.2 Spatial patterns

The grain-size data was plotted on maps for investigating the spatial distribution of the grain size, see Figure 3.7. The results from Run 1, show high values (over 155 µm) on the east and west sides of the map with much lower values (23 to 40 µm) dominating the rest of the map. Run 2 shows predominantly low modal values (23 to 49 µm) over the entire area, but with higher in the northeast near the Hålt delta. Run 3 displays five areas of coarser modal values; three smaller areas in the west, south, and north, as well as two large areas in the central and north-central parts of the map. Together, these form two zones with higher values in an east-west direction. On the other places on the map the value stays between 23-51µm. In run 4 the values are quite uniform, varying from 23 to 51µm.

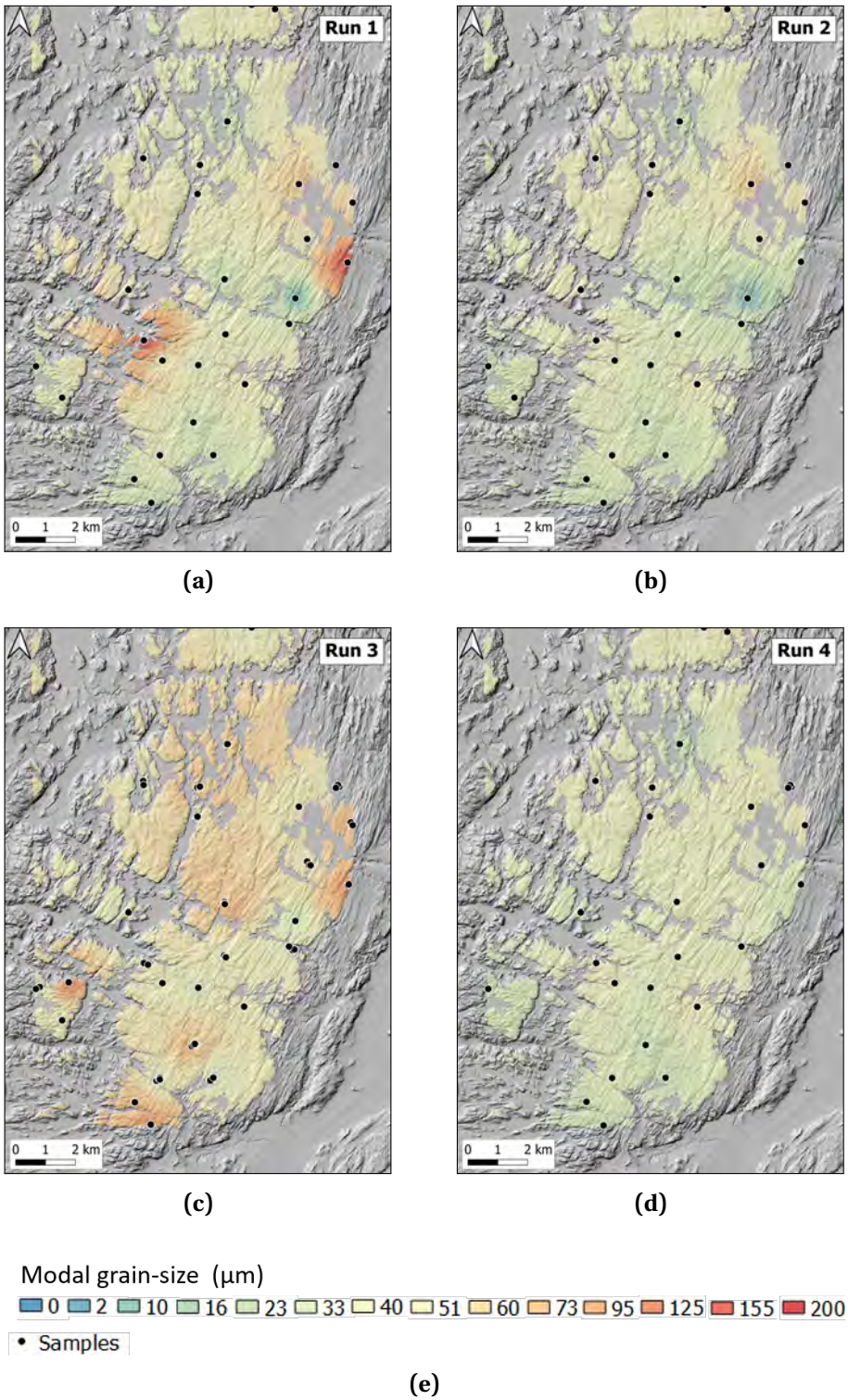

Figure 3.7: Interpolated maps of mode in (a) run 1, (b) run 2, (c) run 3, and (d) run 4. The legend in (e) show the modal values in micrometers and applies to all four maps. © Lantmäteriet Höjdmodell © SGU Highest shoreline

3.1.3 Grain-size analysis - profiles

Sample pits at Torrgårdsvatten, Härsvatten, and Vägen (Figure 3.8, 3.9, 3.10, 3.1) were excavated to view the soil profile. Samples were taken at intervals to analyse the difference in grain-size distribution with depth. The profile from Torrgårdsvatten was visible in a roadside cut and easily cleared (Figure 3.8a). The uppermost 1cm shows a pronounced bimodality, with a primary mode above 500µm with an additional secondary mode around 45µm. All samples have primary modes within the medium and coarse silt ranges apart from the ones taken at 20cm depth and 1cm depth. Though that sample does have a shoulder within the coarse silt fraction, the primary mode consists of fine sand. All samples have fairly similar contents of medium and fine silt, the sample taken at 4cm depth being the exception. This sample has a higher content of finer silts and has the smallest mode value of 30µm. There is no clear connection with changes in mode in relation with depth.

A second profile was analyzed at location Härsvatten (Figure 3.1), in a small depression at the foot of a hill. A 70cm deep sample pit (Figure 3.9a) was dug out in order to clear the profile and samples were taken from every 5cm. The grain-size analysis shown in Figure 3.9b displays mainly unimodal distributions with a coarsening of modal grain-size with depth until 30cm, after which upwards fining occurs. Modal grain-sizes range between 41µm (coarse silt) for the uppermost two layers to 138µm (fine sand) at 30cm depth. The deepest layer has a modal grain size of 52µm. All samples have a shoulder on the fine side, especially pronounced in the deepest two layers. These two have pronounced higher contents of very fine silt then the other layers but fairly similar clay contents. The two upper samples also show a more distinguished peakedness, with kurtosis values of 1.08 and 1.04 bordering on leptokurtic.

(a)

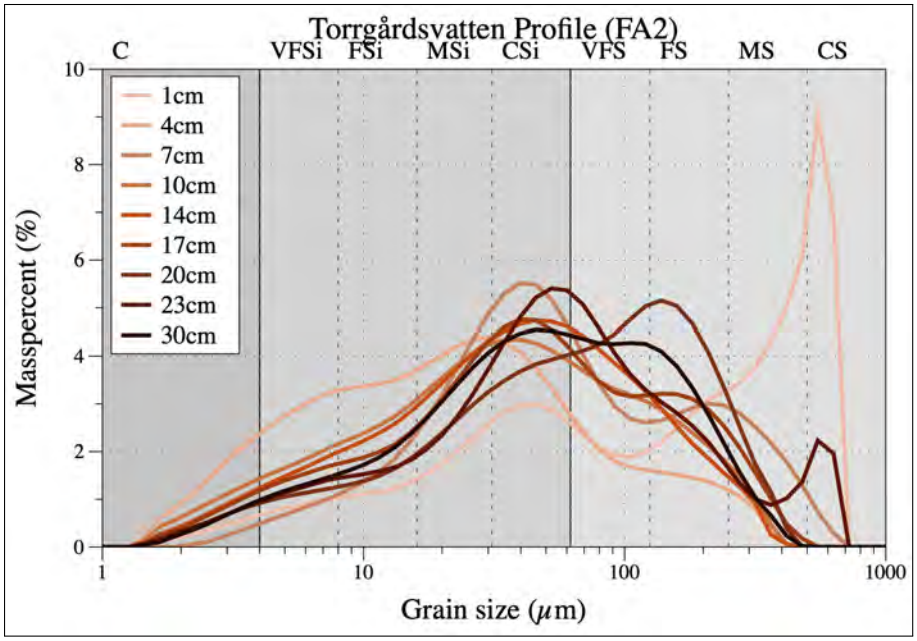

(b)

Figure 3.8: (a) Picture of soil profile at location Torrgårdsvatten, with knife as reference. (b) Grain-size distribution from all profile samples taken at location Torrgårdsvatten.

(a)

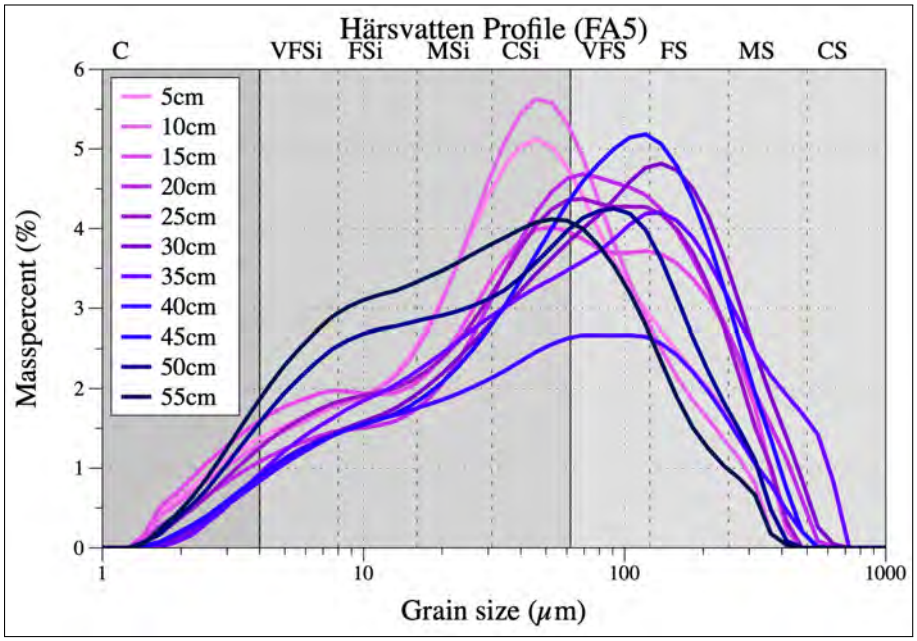

(b)

Figure 3.9: (a) Picture of sample pit by location Härsvatten. (b) Grain-size distribution from all profile samples taken at location Härsvatten.

(a)

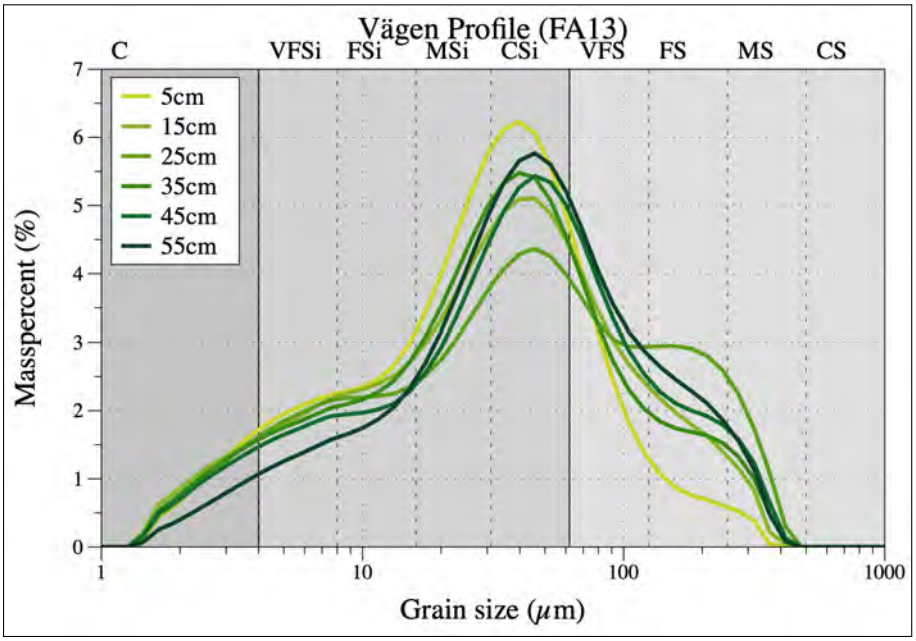

(b)

Figure 3.10: (a) Picture of sample pit by location Vägen. (b) Grain-size distribution from all profile samples taken at location Vägen.

The final sample pit is was dug at Vägen (Figure 3.1). Located just off-center on a high topographic divide, the pit measured 65cm in depth and samples were taken at 5cm intervals. In Figure 3.10a, a grey sandy soil occurs directly on bedrock overlain by the reddish silt-rich layer followed by the organic layer. The modal grain-size values shown in Figure 3.10b all fall within the coarse silt spectrum, varying between 39 and 45µm. All curves show a unimodal appearance with fine-skewness and varying development of coarse shoulders. The most pronounced shoulder is found at 25cm depth where a shoulder within the very fine to fine sand fraction. The sample taken at 5cm depth is most peaked, with a kurtosis value of 1.17 it classifies as leptokurtic. The least peaked sample, the one from 25cm has a kurtosis value of 1.08, i.e. mesokurtic.

3.2 Geochemistry

Geochemistry was investigated in ten samples using p-XRF, the results can be seen in Figure 3.11.

The samples have a silica content of 21wt% to 39wt% and a zirconium and titanium content of 0.2wt% to 1.2%wt. Samples taken from till in the Dösebacka Drumlin have narrower span of values between 31wt% and 39wt% silica content and the substrate samples have values of 21.5wt% to 30.5twt%. The surface silt samples have a larger variation in silica values and varies from 21wt% silica up to 32.5wt%.

For the different grain-sizes from Dösebacka drumlin, the finest sand has a smaller content of zirconium and titanium compared to the coarsest coarse silt, from now on referred to as the coarsest silt. The samples from the surface silt layer do not differentiate much in the zirconium and titanium content but the coarsest silt has more silica comparing to the finest sand. Lastly the substrate samples are fairly similar in zirconium and titanium content except one of the samples. The coarsest silt samples varies between approximately 0.6wt% to 1.2wt%. The finest sand from the substrate have a smaller variation from approximately 0.6wt% up to 0.7%.

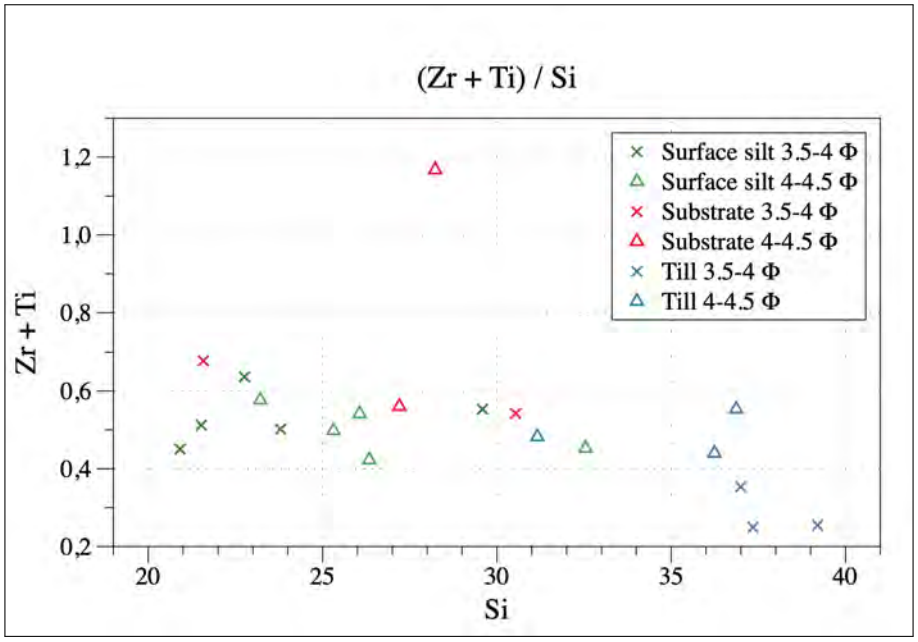

Figure 3.11: Titanitum and zircon in wt% on the y-axis plotted against silica content in wt% on the x-axis. The crosses represents very fine sand and the triangles represents coarse silt.

3.3 Dating

Five samples were taken to be dated in Lund Luminescence Laboratory using optically stimulated luminescence (OSL). One sample (from location Torrgårdsvatten) was taken using the tube method as shown in Figure 2.2c. In the same location one additional sample was taken according to the methodology described in 2.1, which was also used for the remaining four OSL samples taken. The sampling locations are arranged along a north-east to south-west line across the sampling area Figure 3.12. Soil and sample depths for each sampling location is shown in Table 3.2.

Table 3.2: Soil and sample depths for the samples taken for OSL analysis.

Samplin location	Soil depth (cm)	Sample depth (cm)
Torrgårdsvatten 1	30	15
Torrgårdsvatten 2	30	12
Härsvatten (site B)	75	25
Vägen (site B)	65	15
Iglekärr (site B)	45	15

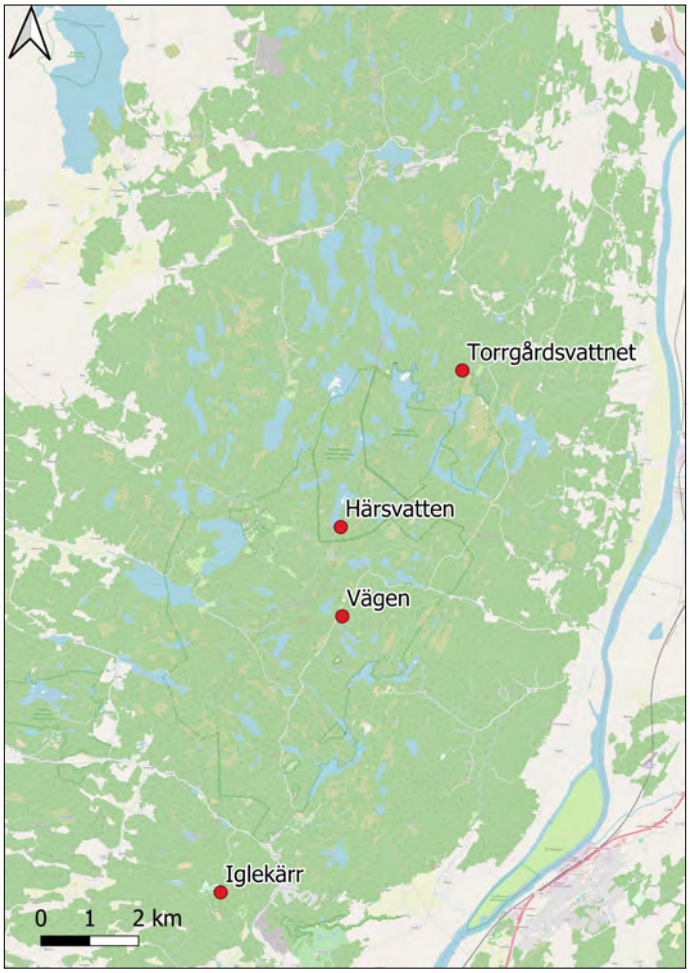

Figure 3.12: Map showing the locations OSL-samples were taken, marked with red dots. © OpenStreetMap contributors, CC-BY-SA

During the OSL-analysis, all samples showed bright signals and relatively tight dose distributions. The analysis generated ages ranging between 1 an 7 ka as shown in Figure 3.13.The timeline includes the age of the Berghem moraine, dated to 14 Cal ka BP according to Stroeven et al. (2016). The report provided by Alexanderson from the OSL analysis can be found in Appendix B.

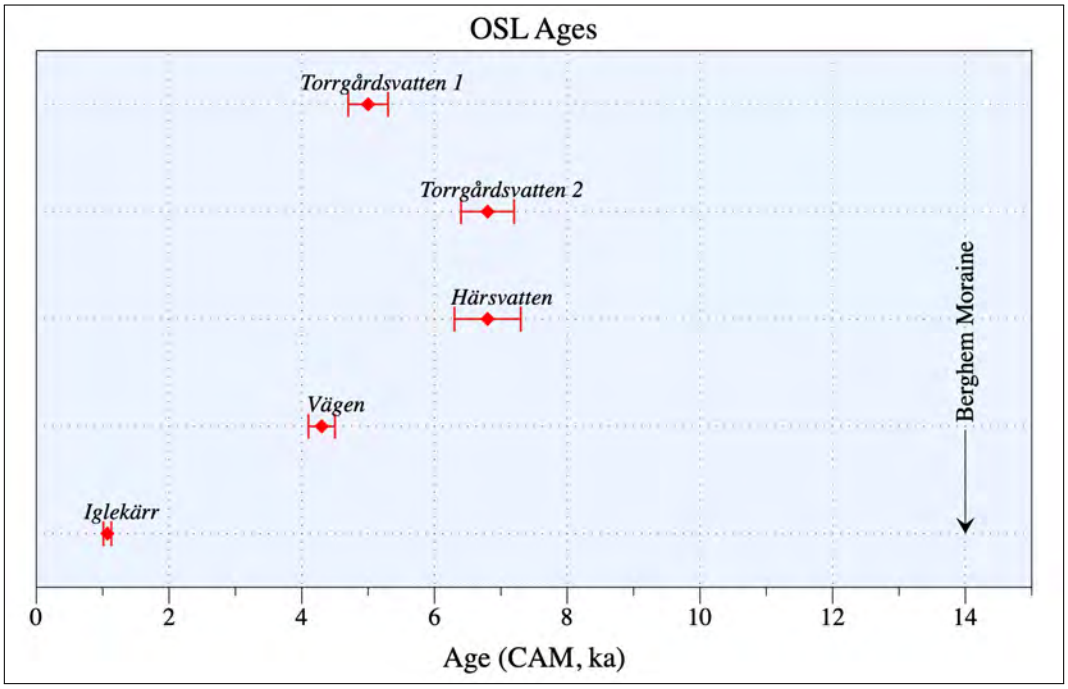

Figure 3.13: Ages with standard deviation derived from OSL-analysis from four locations north to south in falling order. Arrow points out age for the formation of nearby Berghem Moraine at 14 cal ka BP (Stroeven et al., 2016).

4 Discussion

4.1 Is it loess?

In this thesis, loess is defined as a silt-sized windblown sediment. The majority of the layer's modal grain sizes fall within the coarse silt range, but also in the very fine to fine sand. This conforms with other studies of loess in general (Vandenberghe, 2013) and in particular loess in analogue Quaternary settings, such as the thin North-American loess described by Schaetzl & Luehmann (2013) and Schaetzl & Attig (2013). Though loess is commonly well-sorted, this characteristic is not found in the Svartedalen loess. Almost all samples show a primary or secondary mode in the silt fraction agreeing with other studies where similar findings have been interpreted as loess.

Another argument for the layer to be of aeolian origin is its stratigraphic and topographic placement. Located above the highest shoreline, on top of topographic high points and highest up in the stratigraphy leaves few other options as to what it might be if not loess. The layer covers a large area but is irregularly distributed. The thickness is often less on top of topographic high points than topographic lows, which could be explained by topographic lows trapping the silt or silt on the topographic highs is more easily blown or washed away. Slope processes could also be a reason for that thicker deposits can be found at the foot of hills rather than on top. This distribution indicates some slope activity that may have redistributed a primary eolian sediment, but the silt is also found on topographic summits requiring solely eolian deposition.

Other depositional environments that could lead to such a silt-rich deposit are lacustrine, e.g. an ice-dammed lake, a marine environment or a heavily weathered till, as suggested by Svensson (1992). All samples were collected above the highest shoreline to ensure that a marine deposition could be ruled out. Svartedalen is a joint valley landscape and if the valleys were sufficiently blocked by the ice, local ice-dammed lakes could form. As some

samples were taken on topographic highs the plausibility of the genesis being lacustrine is unlikely. This would entail an ice-dammed lake located on the top of a topographic high and could only be created if it was completely surrounded by ice. Furthermore, it is unlikely that all locations have been dammed up and lakes have been created resulting in similar deposition of grain sizes in such a large area as Svartedalen nature reserve; these arguments are also discussed by Svensson (1992). Additionally, ice-dammed lakes do not exclusively deposit silt-sized material and include other facies such as coarser textures and lamination (Donnelly & Harris, 1989; Clayton et al., 2008; Ham & Attig, 2008), which have not been found in Svartedalen during fieldwork.

That the silt-rich layer should have its origin from a till that has been weathered down to the silt fraction is improbable. All older sediments were eroded away during the latest glaciation so therefore the age of the *rödfemma* layer should be post-glacial or earliest syn-glacial. The grain-size distribution of weathered and even highly weathered tills is distinctly different from those of the surface silt (Rovey II & McLouth, 2015; Karlstrom, 2000).

Taking the grain-size modality, history of deglaciation and its geographical as well as stratigraphic placement in the landscape into consideration, there is no other logical explanation of the genesis of this layer than it being of aeolian origin. Thus, the silt-rich soil layer known as *rödfemma* is loess.

4.2 Explanation of textural variations

Though 'ideal' loess is commonly well-sorted, this characteristic is not found in the Svartedalen loess. The presence of coarser material causing bimodality and shoulders is indicative of some kind of mixing, reworking or addition from other processes (i.e. strong winds, slope wash). Other works on thin loess deposits have demonstrated mixing from layers below with the thin loess layer superimposed (Schaetzl & Luehmann, 2013; Schaetzl & Attig, 2013). The grain-size distribution does not follow a specific pattern for all the sites in Svartedalen.

According to Vandenberghe (2013), bimodal samples can indicate reworking from fluvial processes. Slope processes are also something that can lead to a bimodal distribution. In western Transylvania, a bimodal distribution could be seen in a reworked loess-like sediment (Pendea et al., 2009). This was explained as a result of aeolian processes mixing with fluvial slope processes. More examples that are similar to the grain-size distribution of the *rödfemma* layer in Svartedalen are from the northeastern part of Wisconsin (Schaetzl & Luehmann, 2013). Schaetzl & Luehmann (2013) argue that the thin layers is loess mixed with sandier materials from below, and that pedoturbation can act up to 50cm in the soil. As many of the sample locations have thicknesses around 50cm or even less, it is possible to imagine pedoturbation to be an important factor in the *rödfemma* layer. This is especially true in the layers possessing a bimodal grain-size distribution. Not all samples have a bimodality, but a majority have shoulders in the grain-size distribution demonstrating a containment of coarser grains. This pattern can also be seen in Schaetzl & Luehmann (2013), where shoulders are present. A point of interest is the occurrence of the fine shoulders present in many of the samples, which was not expected. If this is a result of aeolian clay being transported in separate particles, particle clusters or post-depositional weathering is unclear. Although mixing is a reasonable cause for the variations seen in the grain-size distributions, there is little evidence for abundant sub-loess sediment. All sites are on bedrock, and if coarser material is present between the loess and bedrock, it is in all places thin (10-15 cm). The grain-size distribution indicates some kind of reworking which could either be syn- or postdepositional to the original event creating the *rödfemma* layer.

The profile from location Vägen (Figure 3.10) indicates primary aeolian deposition as the distribution curves have a better fit between each other and there is generally quite a low presence of sand. The one exception being the layer from 25cm depth which contained a shoulder of fine sand. The samples from the profile were collected from the top of a ridge, which could then indicate that there has been little reworking from slope-processes. This could certainly be a result of reworking by slope processes and pedoturbation, but it seems likelier that a different factor is at play. Is this a result of a sudden increased wind strength, a period of stronger winds enabling saltating fine sands to reach further afield from the source? Or is it maybe due to a shift in sources? The activation of a closer located deposit, making it

possible for sands to reach the sample areas? Location Ålevatten (Figure 3.3c) shows the two separate modes for sample B and its substrate combined in the A sample, an indication of mixing. The profile from location Härsvatten (Figure 3.9) have a larger variance which could reflect more pedoturbation in addition or alternative to slope processes. This profile is situated at a depression at the foot of a hill and during fieldwork boulders and cobbles incorporated into the layer was noticed when a sample pit was dug. The occurrence of these larger objects can be explained by slope processes during the deposition. Alternatively the object could have been incorporated after the deposition of the silt by pedoturbation.

The modal grain sizes are predominantly in the coarse silt fraction which according to Vandenberghe (2013) indicates transportation in suspension near the ground surface with a relative short travel distances of tens of kilometers. Further, Vandenberghe argues that the difference in wind-strength and local topography can influence the variation in this group. Some samples have coarser silt or fine sand modal grain sizes, indicating shorter transport distances according to Vandenberghe (2013). Mode of transport can be saltation or low suspension clouds near the surface, but is mostly depending on the availability of source material. One sample consists of very fine silt which is transported in high suspension clouds (Vandenberghe, 2013).

4.3 Possible sources and paleowind direction

Grain size and its spatial variation can be indicative of its source, as normally both the texture and thickness of aeolian material decrease downwind (Smith, 1942; Mason, 2001). Svensson (1992) suggested the ice-marginal delta of Hålt as a potential source for the *rödfemma* layer in Svartedalen. This was based on grain-size data collected during the study, as shown in Figure 4.1.

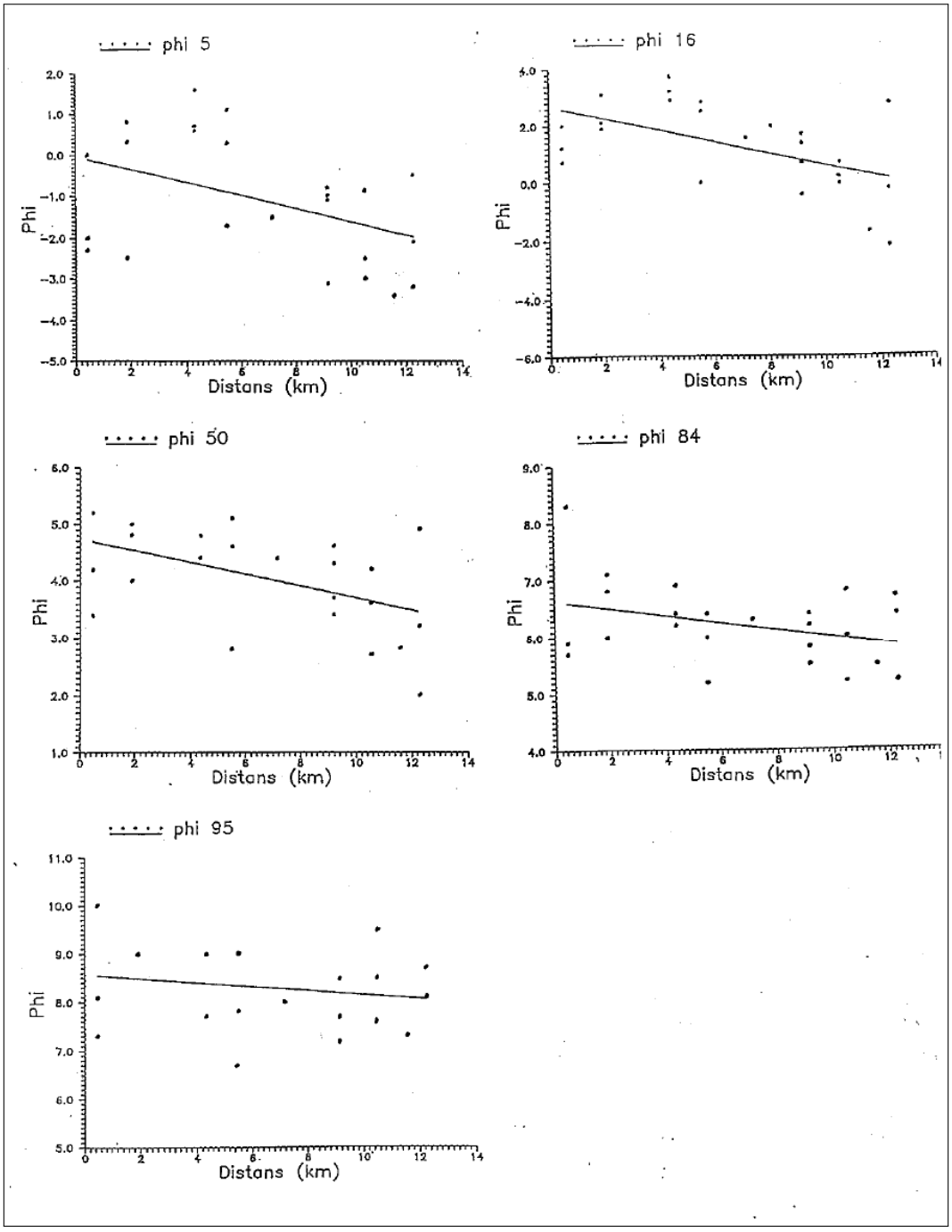

Figure 4.1: Results from (Svensson, 1992), showing trends in grain-size distribution spatially in different grain-size percentiles.

The diagrams in Figure 4.1 show the variation in grain sizes for different phi-percentiles in relation to distance from the Hålt delta. Svensson states that the diagrams show a higher degree of coarser grains further away from Hålt but also that the finest grain-sizes of each sample were smaller with distance. Svensson discussed that the higher quantity of fines found near Hålt and larger grain sizes further away could be explained by that the samples further away had thinner layers and more mixing of substrate with the finer fines. This trend described by Svensson (1992) could not be reproduced in this thesis as no spatial pattern could support this when sampling a significantly larger study area, shown in Figure 3.7.

A previous idea was that aeolian sediments were deposited by katabatic winds contemporaneous or penecontemporaneous to the deglaciation in Fennoscandia (Högbom (1913) in Bernhardson & Alexanderson (2018)) (Högbom, 1923; Hörner, 1927; Hjulström et al., 1955). Contradictory to this, it has been shown that the katabatic winds have a small to no influence for the formation of the aeolian sand dunes during the deglaciation (Bernhardson & Alexanderson, 2018; Bernhardson et al., 2019). According to Bernhardson et al. (2019) paleowind directions in south-central Sweden were mainly westerly and northwesterly. This is not coherent with the spatial distribution maps produced in this thesis as they show no apparent wind-direction pattern. As seen in Figure 3.7a-c several areas displaying coarser modal distributions are present, this could be indicative of wind patterns. The southern part in Figure 3.7a fits with the westerly and northwesterly winds suggested by Bernhardson et al. (2019). But as the silt-rich layer is indicative of mixing it is likely that the spatial patterns is a misleading result of this mixing. Instead we suggest a multiple source option. We conclude that the lack of spatial patterns in grain-size and geochemical information does not support the notion of a single point source for the wind-deposited silt.

Rödfemma does not appear to be unique for Svartedalen nature reserve. It has been described in soil-map descriptions produced by the Swedish geological survey as well as anecdotal field observations communicated to the authors by experienced geologists (personal communication, T. Påsse 2020-03-02). The Hålt delta as the point source for the soil found in Svartedalen, much less all *rödfemma* within the region beyond Svartedalen, appears unlikely due to its relatively insignificant size and placement. Deflation of glacial and non-glacial deposits is a well-known occurring process and the source of loess (Schaetzl

& Luehmann, 2013; Grimley, 2000). Given the abundance of large such accretions that surround the study area such as Dösebacka, Ucklum and Lysegården, it is not implausible that multiple sources could be at play. Whether these multiple sources were actively deflating and transporting silt to Svartedalen simultaneously or consecutively is unclear. Another possible source would be from the ice sheet itself.

Provenance is not a topic that has been looked at in this study, however, given the placement the region would have had under the massive ice sheet, the bedrock origin is likely fairly local. This area would have been in the erosional zone of the ice sheet for a majority of its duration, meaning that any till found here would have been deposited as the ice retreated. Kleman et al. (2008) states that long-distance transport primarily occurs during the expansive phase of the ice sheet, from which we can draw the conclusion that retreating phase deposited material would not have been derived far away. This is supported by unpublished data verbally communicated by Thomas Stevens, associate professor at Uppsala University. Stevens joined the authors in the field and took a sample at location Torrgårdsvatten in order to conduct U/Pb dating. Presenting these unpublished results, the dated zircons all showed a united peak around 1.6 billion years ago, coinciding neatly with the already known bedrock ages of the Idefjorden terrane created during the Gothian orogeny.

4.4 Geochemistry

The variation in the geochemistry results were not significant and the results from Schaetzl & Loope (2008) could not be reproduced for the Svartedalen study area. The hypothesis for the results was that there would be less heavy minerals in the coarsest fraction than in the finest fraction as a result of the transportation by wind, as Schaetzl & Loope (2008) showed for the thin North American loess. Additionally, it was believed that the heavy minerals would be evenly distributed over the grain-size fractions in the till from Dösebacka, i.e. no sorting would occur. The results do not show a pattern within the grain-size fraction. The results from the handheld p-XRF were calculated based on ratios and it is crucial that these ratios

from the CRMs are correct as the samples have such small amounts to be detected. The best effect for analyzing samples is to grind them (Gallhofer & Lottermoser, 2020) which was not done for this study, but the samples were homogenized in the same grain size which should minimize the source of errors. Still, this is something that can effect the results and the margin of error. Another factor that can impact the results is that titanium can be a component in other minerals than the heavies, such as biotite. Biotite is easily transported by the wind which can result in an increased inclusion of titanium in the larger grain-size fractions. However, the titanium found in biotite can also result in an over-representation of titanium in the small grain-size fractions as biotite weathers more easily than rutile, zircon and titanite. Looking on zirconium alone might be a better proxy for heavy minerals as to avoid the misrepresentation of titanium.

4.5 Timing

The absolute maximum age that the silt-rich layer would be penecontemporaneous to the retreat of the ice sheet from the area about 14 cal ky BP (Stroeven et al., 2016). This is due to the efficient erosion of the immense ice sheet which, apart from a thin layer of till, left the landscape bare after receding. Episodes of high aeolian activity are described in Bernhardson et al. (2019), where sand dunes in central Sweden were dated to have been last active between 10.5 and 9.5 ka BP as well as between 4 and 2 ka BP. Bernhardson & Alexanderson (2018) also found active sand dunes in mid-Sweden dated between 10.5 and 7.2 ka BP. The OSL-dating results provided lower ages than these, ranging between 6.8 and 1.07 ka. The older of these do coincide with a period of increased dustiness in south-central Sweden, as described by Kylander et al. (2013) based on analysed bog cores.

The dates derived from OSL-analysis show the date when the grain was last exposed to sunlight, e.g. when it was buried. Our original hypothesis was that the age of the loess would be immediately after deglaciation when sediment sources (outwash surfaces) were active and devoid of vegetation. The ice itself may have been a source, requiring its proximity. However, the dates are much younger than the date of deglaciation. Do these dates reflect

the time of deposition by wind or are they in fact a result of bleaching due to post-depositional mixing, which already has been established as a likely process to have occurred? In order for deflation of glaciofluvial deposits to happen, the surface must be free from vegetation that acts as a binding agent. This could have happened during arid times between the retreat of the ice sheet and present day, but would definitely been the case after the retreat. The thin nature of the silt-rich layer could also have an effect on the results. Professor R. Schaetzl, who has studied thin loess deposits in North America, has through personal communication (2021-05-10) expressed that loess layers of lower thickness than 1.5m result in too low ages when dated by OSL. This he explains as likely caused by bioturbation bleaching the dated quartz grains as they are brought up to the surface. As all OSL-samples for this thesis were taken at a depth of 0.25m or less, and mixing of the samples likely has occurred due to pedoturbation, this could be an explanation of the lower than expected ages derived from this study.

The methodology when performing the OSL-analysis and calculation for dating the samples also has an impact on the results. When writing this thesis, Alexanderson retested the sample Torrgårdsvatten 2 with a different method of OSL-analysis where a smaller aliquot of grains were tested and dated by a maximum age model. Using aliquots and not single grain analysis means that the result is a mean value from all grains found within the aliquot. Should there be a variation in ages within these grains due to mixing, the mean value would be lower than the grain which has spent the longest time buried. The smaller aliquot means that there are less grains affecting the mean age value and the statistical model provides the date for the oldest date derived from the analysis. This analysis provided an age of 11.2 ka BP with a standard deviation of 0.8 ka BP, which is closer to the hypothesized values than the 6.8 ka BP presented in the results. This sample was taken directly above bedrock with no till layer in between, which indicates that the age of the burial comes from grains within the actual loess layer. The age of 11.2 ka BP also fits better with the ages of 10.5-9.5 provided by Bernhardson et al. (2019).

As mentioned previously, deposition could have its origin in multiple sources. Would one source have been able to cover the entirety of Svartedalen in one go, or do different areas within Svartedalen have separate sources? As the ages of the glacial deposits depend on the ice margin placement, the time of deflation would have varied accordingly. Thus, sources

could have shifted during deposition depending on which was then actively deflating, causing layers within the *rödfemma* to have different origins. Deposition would not have been the result of a one-time event, but rather time-transient.

4.6 Suggestions for further studies

Suggestions for further studies to investigate the silt-rich layer *rödfemman* involve a more developed OSL sampling and analysis campaign. New OSL-samples should be taken at sites where the soil depths are deeper, for example at sample location Vägen. A sample pit should be dug out from where the OSL-sample can be taken horizontally. The method used by Alexanderson to re-date one sample simultaneously as this thesis was being written should be further explored and applied for the dating. The geochemical composition of the layer could also be further investigated, perhaps by mapping the amount of dense grains in the sample with a SEM-EDS. This could give a more accurate representation of the ratio of heavies and perhaps show spatial variations which were not found in this study. Additionally, the grain-surface texture could be investigated with the SEM-EDS which could give further indications of the depositional environment. The chain of depositional events could be made clearer by creating more soil profiles.

5 Conclusions

- From the grain-size distribution, it is clear that the majority of samples have modal values in the silt fraction, primarily in the coarse silt fraction. Together with other factors, such as the study area's situation above the highest shoreline, on topographic highs and the large spatial distribution, we argue that the silt-rich layer, colloquially known as *rödfemman*, has an aeolian genesis and therefore is loess.

- The grain-size distribution is not always unimodal, some samples are bimodal or unimodal with a shoulder in the coarse fraction and some samples have pure bimodal distributions. We argue that this is a result of reworking or mixing by pedoturbation and/or slope processes. This implies that some of the samples are secondary loess and not a primary loess. Type of reworking process could vary from location to location as the depositional conditions are highly effected by topography.

- A possible source and wind direction was investigated by looking on aerial distribution of the mode. No spatial patterns were evident from this and therefore no specific source could be determined. A suggestion is multiple sources resulting in the lack of spatial pattern, alternatively reworking or mixing that has interfered with the patterns.

- Maximum age of deposition should coincide with the deglaciation. The OSL-dating provides minimum ages for when the silt-rich layer was buried of 6.8-1.08 ka BP. These dates could either represent the date of deposition or an indication of post-depositional bleaching due to pedoturbation. The reassessment of one sample indicates that grains with older burial ages do exist within the sample, which implies earlier deposition.

6 Bibliography

Agrell, H., & Hultman, R. (1971). Deposits of wind-blown silt in the north-eastern part of the southern swedish uplands. *GFF*, *93*(1), 231-235. Retrieved from https://www.scopus.com/inward/record.uri?eid=2-s2.0-84950718537&doi=10.1080%2f11035897109451941&partnerID=40&md5=ef0f885b32b094c819069febbbf307d6 doi: 10.1080/11035897109451941

Bernhardson, M., & Alexanderson, H. (2018). Early holocene nw-w winds reconstructed from small dune fields, central sweden. *Boreas*, *47*(3), 869-883. doi: 10.1111/bor.12307

Bernhardson, M., Alexanderson, H., Björck, S., & Adolphi, F. (2019). Sand drift events and surface winds in south-central sweden: From the deglaciation to the present. *Quaternary Science Reviews*, *209*, 13-22. doi: 10.1016/j.quascirev.2019.01.017

Björsjö, N. (1949). *Israndsstudier i södra bohuslän* (Vol. 42) (No. 2). Stockholm: SGU.

Clark, P. U., Dyke, A. S., Shakun, J. D., Carlson, A. E., Clark, J., Wohlfarth, B., ... McCabe, A. M. (2009). The last glacial maximum. *Science*, *325*(5941), 710-714. Retrieved from https://dx.doi.org/10.1126/science.1172873 doi: 10.1126/science.1172873

Clayton, L., Attig, J. W., Ham, N. R., Johnson, M. D., Jennings, C. E., & Syverson, K. M. (2008). Ice-walled-lake plains: Implications for the origin of hummocky glacial topography in middle north america [Journal Article]. *Geomorphology*, *97*(1-2), 237-248. Retrieved from https://dx.doi.org/10.1016/j.geomorph.2007.02.045 doi: 10.1016/j.geomorph.2007.02.045

Donnelly, R., & Harris, C. (1989). Sedimentology and origin of deposits from a small ice-dammed lake, leirbreen, norway. *Sedimentology*, *36*(4), 581-600. Retrieved from https://www.scopus.com/inward/record.uri?eid=2-s2.0-0024827879&doi=10.1111%2fj.1365-3091.1989.tb02087.x&partnerID=40&md5=8c51531d186eca24fb055152651a005b (cited By 28) doi: 10.1111/j.1365-3091.1989.tb02087.x

Ehlers, J., & Gibbard, P. L. (2004). *Quaternary glaciations : extent and chronology. p. 1, europe* (1. ed. ed.). Amsterdam: Amsterdam : Elsevier.

Enquist, F. (1932). The relation between dune-form and wind-direction. *Geologiska Föreningen i Stockholm Förhandlingar*, *54*(1), 19-59.

Fjeldskaar, W. (1991). Geoidal-eustatic changes induced by the deglaciation of fennoscandia. *Quaternary International*, *9*, 1-6.

Folk, R. L., & Ward, W. C. (1957). Brazos river bar [texas]; a study in the significance of grain size parameters [Journal Article]. *Journal of Sedimentary Research*, *27*(1), 3-26.

Fredén, C. (1986). *Beskrivning till jordartskartan göteborg no* (40th ed., Vol. Ae) (No. 40). Uppsala: SGU.

Fredén, C. (1987). *Jordartskartan 7a marstrand no/7b göteborg nv. beskrivning* (63rd ed.). Uppsala: SGU.

Fredén, C. (1997). *Beskrivning till jordartskartan borås nv* (40th ed., Vol. Ae) (No. 114). Uppsala: SGU.

Fredén, C. (2001). *Beskrivning av jordartskartan 11d munkfors so* (Vol. 150) (No. Ae). Östervåla: SGU.

Gallhofer, D., & Lottermoser, B. (2020). The application of pxrf for the chemical and mineralogical characterization of heavy mineral sands. *Geochemistry: Exploration, Environment, Analysis*, *20*(1), 99–111.

Grimley, D. A. (2000). Glacial and nonglacial sediment contributions to wisconsin episode loess in the central united states. *Bulletin of the Geological Society of America*, *112*(10), 1475-1495. Retrieved from https://www.scopus.com/inward/record.uri?eid=2-s2.0-84879885477&doi=10.1130%2f0016-7606%282000%29112%3c1475%3aGANSCT%3e2.0.CO%3b2&partnerID=40&md5=96ae938a785e6afb62ce4344f7f6f95b doi: 10.1130/0016-7606(2000)112<1475:GANSCT>2.0.CO;2

Ham, N. R., & Attig, J. W. (2008). Ice wastage and landscape evolution along the southern margin of the laurentide ice sheet, north-central wisconsin [Journal Article]. *Boreas*, *25*(3), 171-186. Retrieved from https://dx.doi.org/10.1111/j.1502-3885.1996.tb00846.x doi: 10.1111/j.1502-3885.1996.tb00846.x

Hillefors, (1969). *Västsveriges glaciala historia och morfologi : naturgeografiska studier* (Unpublished doctoral dissertation). Diss. Lund : Univ., Lund

Hjulström, F., Sundborg, , & Falk, (1955). Problems concerning the deposits of windblown silt in sweden. *Geografiska Annaler*, *1-2*, 86-117.

Högbom, I. (1913). Finiglaziale flugsandfelder in dalarne. *Geologiska Föreningen i Stockholm Förhandlingar*, *35*(7), 484–500.

Högbom, I. (1923). Ancient inland dunes of northern and middle europe. *Geografiska Annaler*, *5*(2-3), 113–242.

Hörner, N. G. (1927). *Brattforsheden ett värmländskt randdeltakompex och dess dyner* (Vol. 20) (No. 3). Stockholm: Kungl. Boktryckeriet. P.A. Nordstedt Söner.

Johansson, B. (1982). *Deglaciationen av norra bohuslän och södra dalsland* . Geologiska Instutionen.

Karlstrom, E. T. (2000). Use of soils to identify glacial deposits of various ages east of glacier national park, montana, usa. *Arctic, Antarctic, and Alpine Research*, *32*(2), 179–188.

Kleman, J., Stroeven, A. P., & Lundqvist, J. (2008). Patterns of quaternary ice sheet erosion and deposition in fennoscandia and a theoretical framework for explanation. *Geomorphology*, *97*(1), 73-90. Retrieved from https://www.sciencedirect.com/science/article/pii/S0169555X07002863 (Glacial Landscape Evolution - Implications for Glacial Processes, Patterns and Reconstructions) doi: https://doi.org/10.1016/j.geomorph.2007.02.049

Kylander, M. E., Bindler, R., Cortizas, A. M., Gallagher, K., Mörth, C.-M., & Rauch, S. (2013). A novel geochemical approach to paleorecords of dust deposition and effective humidity: 8500 years of peat accumulation at store mosse (the “great bog”), sweden [Journal Article].

Quaternary Science Reviews, *69*, 69-82. Retrieved from https://dx.doi.org/10.1016/j.quascirev.2013.02.010 doi: 10.1016/j.quascirev.2013.02.010

Lidmar-Bergström, K. (1995). Relief and saprolites through time on the baltic shield. *Geomorphology*, *12*(1), 45-61. Retrieved from https://www.sciencedirect.com/science/article/pii/0169555X94000764 doi: https://doi.org/10.1016/0169-555X(94)00076-4

Lidmar-Bergström, K. (1996). Long term morphotectonic evolution in sweden. *Geomorphology*, *16*(1 SPEC. ISS.), 33-35. Retrieved from https://www.scopus.com/inward/record.uri?eid=2-s2.0-0029753742&doi=10.1016%2f0169-555X%2895%2900083-H&partnerID=40&md5=6dc06422638f602cdc4d55b7ad93d052 (cited By 119) doi: 10.1016/0169-555X(95)00083-H

Lundqvist, I. (1997). *Berggrundskartan 6b kungsbacka so. beskrivning till berggrundskartan kungsbacka so.* Uppsala: SGU.

Magnusson, E., & Lundegårdh, P. (1972). *Beskrivning till geologiska kartbladet Örebro so* (40th ed., Vol. Ae) (No. 8). Stockholm: SGU.

Mahowald, N., Baker, A., Bergametti, G., Brooks, N., Duce, R., Jickells, T., … Tegen, I. (2005). Atmospheric global dust cycle and iron inputs to the ocean. *Global Biogeochemical Cycles*, *19*(4). Retrieved from https://www.scopus.com/inward/record.uri?eid=2-s2.0-31344479792&doi=10.1029%2f2004GB002402&partnerID=40&md5=2370f85a41e43fb0e66b82faa32343c2 (cited By 729) doi: 10.1029/2004GB002402

Malvern, I. L. (1997). *Manual: Mastersizer sx getting started issue 1.3* (Manual).

Marković, S., Bokhorst, M., Vandenberghe, J., McCoy, W., Oches, E., Hambach, U., … Machallet, B. (2008). Late pleistocene loess-palaeosol sequences in the vojvodina region, north serbia. *Journal of Quaternary Science*, *23*(1), 73-84. Retrieved from https://www.scopus.com/inward/record.uri?eid=2-s2.0-38749097019&doi=10.1002%2fjqs.1124&partnerID=40&md5=01a7bdab39c34603754d6c5b52fd60b0 (cited By 199) doi: 10.1002/jqs.1124

Mason, J. A. (2001). Transport direction of peoria loess in nebraska and implications for loess sources on the central great plains. *Quaternary Research*, *56*(1), 79-86. Retrieved from https://www.sciencedirect.com/science/article/pii/S0033589401922501 doi: https://doi.org/10.1006/qres.2001.2250

Miller, R. L., Knippertz, P., García-Pando, C. P., Perlwitz, J. P., & Tegen, I. (2014). Impact of dust radiative forcing upon climate. In *Mineral dust* (pp. 327–357). Springer.

Muhs, D. R., & Bettis, E. A. (2003). *Quaternary loess-paleosol sequences as examples of climate-driven sedimentary extremes* (Vol. 370). U.S. Geological Survey, MS 980, Federal Center, Box 25046, Denver, CO 80225, United States Department of Geoscience, University of Iowa, Iowa City, IA 52242, United States: Geological Society of America. Retrieved from https://www.scopus.com/inward/record.uri?eid=2-s2.0-84862014372&doi=10.1130%2f0-8137-2370-1.53&partnerID=40&md5=79f98f13f0cf7a6c7cc24f6e5f47a2cd doi: 10.1130/0-8137-2370-1.53

Muhs, D. R., Cattle, S. R., Crouvi, O., R., D.-D., Sun, J., & Zárate, M. A. (2014). Loess records [Book Section]. In *Mineral dust* (p. 411-441). Springer.

Mörner, N.-A. (1969). *The late quaternary history of the kattegatt sea and the swedish west coast : deglaciation, shorelevel displacement, chronology, isostasy and eustasy.* Stockholm: Stockholm.

Mörner, N.-A. (1971). Eustatic changes during the last 20,000 years and a method of separating the isostatic and eustatic factors in an uplifted area. *Palaeogeography, Palaeoclimatology, Palaeoecology*, *9*(3), 153-181.

Mörner, N.-A. (1972). Isostasy, eustasy and crustal sensitivity. *Tellus*, *24*(6), 586-592. Retrieved from https://dx.doi.org/10.3402/tellusa.v24i6.10687 doi: 10.3402/tellusa.v24i6.10687

Okin, G., Mahowald, N., Chadwick, O., & Artaxo, P. (2004). Impact of desert dust on the biogeochemistry of phosphorus in terrestrial ecosystems. *Global Biogeochemical Cycles*, *18*(2), GB2005 1-9. Retrieved from https://www.scopus.com/inward/record

.uri?eid=2-s2.0-4844230127&doi=10.1029%2f2003GB002145&partnerID=40&md5=3ead3bc0d0bb703ed3fbab7035522a01 (cited By 282) doi: 10.1029/2003GB002145

Olympus. (2015). *Delta family handheld xrf analyzers usenr's manual* (Manual).

Pendea, I., Gray, J., Ghaleb, B., Tantau, I., Badarau, A., & Nicorici, C. (2009). Episodic build-up of alluvial fan deposits during the weichselian pleniglacial in the western transylvanian basin, romania and their paleoenvironmental significance. *Quaternary International*, *198*(1-2), 98-112. Retrieved from https://www.scopus.com/inward/record.uri?eid=2-s2.0-62749097313&doi=10.1016%2fj.quaint.2008.05.002&partnerID=40&md5=56c31b8bca5d8a563a03e0ca39b4ea76 (cited By 10) doi: 10.1016/j.quaint.2008.05.002

Petersson, A., Scherstén, A., Bingen, B., Gerdes, A., & Whitehouse, M. J. (2015). Mesoproterozoic continental growth: U–pb–hf–o zircon record in the idefjorden terrane, sveconorwegian orogen. *Precambrian Research*, *261*, 75–95.

Prothero, D. R. (2014). *Sedimentary geology : an introduction to sedimentary rocks and stratigraphy* (Third edition. ed.) [Book]. New York : W.H. Freeman.

Påsse, T. (1996). *A mathematical model of the shore level displacement in fennoscandia* (Tech. Rep.).

Påsse, T., & Andersson, L. (2005). Shore-level displacement in fennoscandia calculated from empirical data. *GFF*, *127*(4), 253-268. Retrieved from https://dx.doi.org/10.1080/11035890501274253 doi: 10.1080/11035890501274253

Pécsi, M. (1990). Loess is not just the accumulation of dust [Journal Article]. , *7*, 1-21.

Rhodes, E. (2011). Optically stimulated luminescence dating of sediments over the past 200,000 years. *Annual Review of Earth and Planetary Sciences*, *39*, 461-488. Retrieved from https://www.scopus.com/inward/record.uri?eid=2-s2.0-79955520501&doi=10.1146%2fannurev-earth-040610-133425&partnerID=40&md5=d8a6b7490704f2f1b16cf1cf28181b9a (cited By 239) doi: 10.1146/annurev-earth-040610-133425

Rovey II, C., & McLouth, T. (2015). A near synthesis of pre-illinoian till stratigraphy in the central united states: Iowa, nebraska and missouri. *Quaternary Science Reviews*, *126*, 96–111.

Schaetzl, R. J., & Attig, J. W. (2013). The loess cover of northeastern wisconsin. *Quaternary Research*, *79*(2), 199-214. doi: 10.1016/j.yqres.2012.12.004

Schaetzl, R. J., Bettis, E. A., Crouvi, O., Fitzsimmons, K. E., Grimley, D. A., Hambach, U., … Zech, R. (2018). Approaches and challenges to the study of loess–introduction to the loessfest special issue. *Quaternary Research*, *89*(3), 563-618. Retrieved from https://dx.doi.org/10.1017/qua.2018.15 doi: 10.1017/qua.2018.15

Schaetzl, R. J., & Loope, W. L. (2008). Evidence for an eolian origin for the silt-enriched soil mantles on the glaciated uplands of eastern upper michigan, usa. *Geomorphology*, *100*(3-4), 285-295. Retrieved from https://www.scopus.com/inward/record.uri?eid=2-s2.0-48749102780&doi=10.1016%2fj.geomorph.2008.01.002&partnerID=40&md5=916206345a1e57298fbc44d8bb0cf972 doi: 10.1016/j.geomorph.2008.01.002

Schaetzl, R. J., & Luehmann, M. D. (2013). Coarse-textured basal zones in thin loess deposits: Products of sediment mixing and/or paleoenvironmental change? *Geoderma*, *192*, 277-285.

Smalley, I., Marković, S. B., & Svirčev, Z. (2011). Loess is [almost totally formed by] the accumulation of dust [Journal Article]. *Quaternary international*, *240*(1), 4-11. doi: 10.1016/j.quaint.2010.07.011

Smith, G. D. (1942). Illinois loess: variations in its properties and distribution, a pedologic interpretation. *Bulletin (University of Illinois (Urbana-Champaign campus). Agricultural Experiment Station); no. 490*.

Sprafke, T., & Obreht, I. (2016). Loess: Rock, sediment or soil - what is missing for its definition? *Quaternary International*, *399*, 198-207. Retrieved from https://www.scopus.com/inward/record.uri?eid=2-s2.0-84928536720&doi=10.1016%2fj.quaint.2015.03.033&partnerID=40&md5=755959a620af8231912d9f82e907a887 doi: 10.1016/j.quaint.2015.03.033

Stevens, T., Marković, S., Zech, M., Hambach, U., & Sümegi, P. (2011). Dust deposition and climate in the carpathian basin over an independently dated last glacial-interglacial cycle. *Quaternary Science Reviews*, *30*(5-6), 662-681. Retrieved from https://www.scopus.com/inward/record.uri?eid=2-s2.0-79952042448&doi=10.1016%2fj.quascirev.2010.12.011&partnerID=40&md5=29b1a1617509cd82ebe9d7db8651b93e (cited By 172) doi: 10.1016/j.quascirev.2010.12.011

Stroeven, A. P., Hättestrand, C., Kleman, J., Heyman, J., Fabel, D., Fredin, O., … Jansson, K. N. (2016). Deglaciation of fennoscandia. *Quaternary Science Reviews*, *147*(C), 91-121. doi: 10.1016/j.quascirev.2015.09.016

Sturkell, E., & Hegardt, E. (2020). *Regional geology in gothenburg area.*

Svendsen, J. (2004). Late quaternary ice sheet history of northern eurasia. *Quaternary Science Reviews*, *23*(11-13), 1229-1271. Retrieved from https://dx.doi.org/10.1016/j.quascirev.2003.12.008 doi: 10.1016/j.quascirev.2003.12.008

Svensson, B. (1992). *Undersökning av finjord ovan hk i svartedalen, södra bohuslän, med frågeställning: Eolisk genes* (Unpublished doctoral dissertation). Göteborgs Universitet och Chalmers Tekniska Högskola, Gothenburg.

Vandenberghe, J. (2013). Grain size of fine-grained windblown sediment: A powerful proxy for process identification. *Earth-Science Reviews*, *121*, 18–30. doi: https://doi.org/10.1016/j.earscirev.2013.03.001

A Appendix

A.1 Appendix A

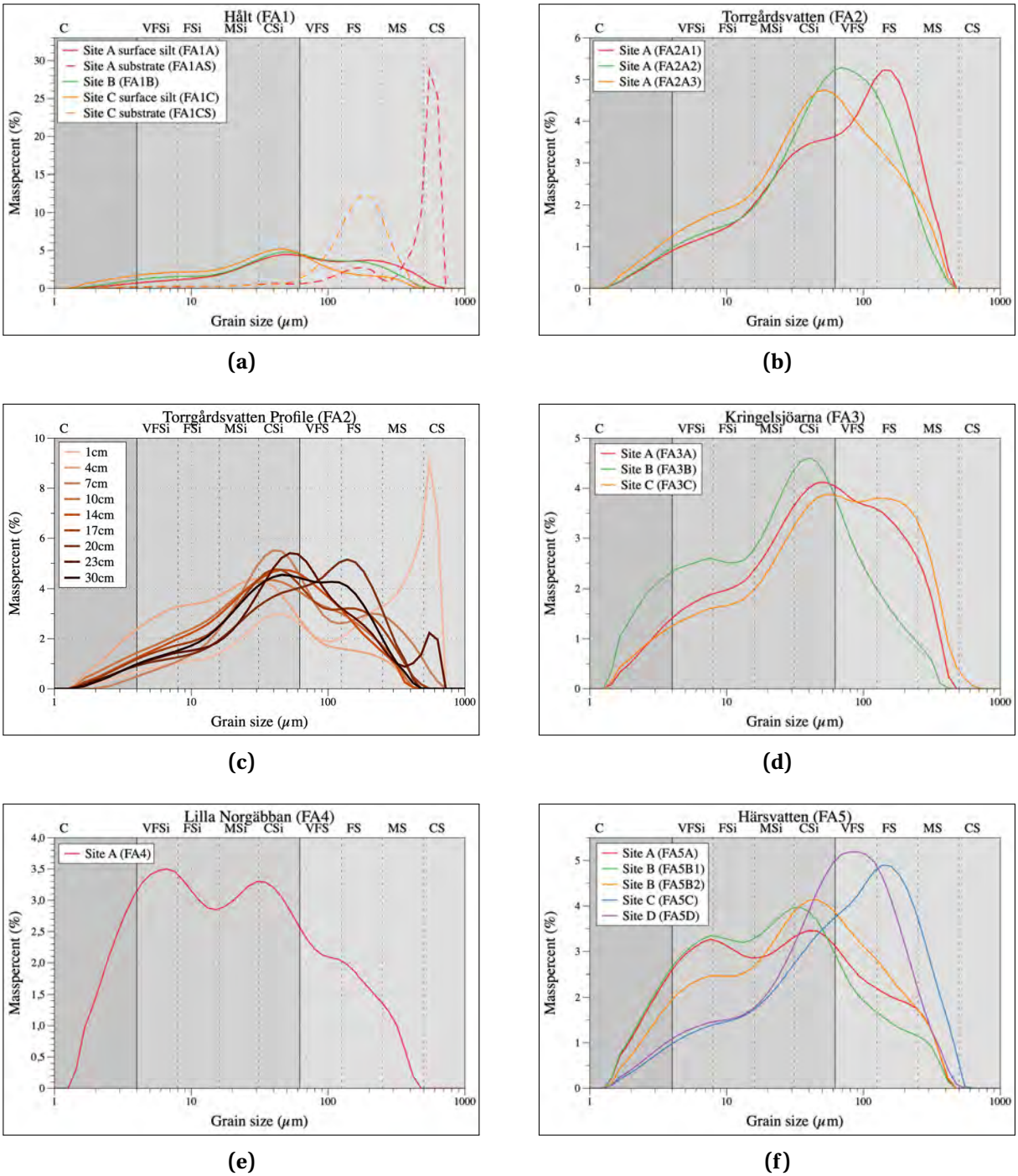

Figure A.1: Grain-size distributions

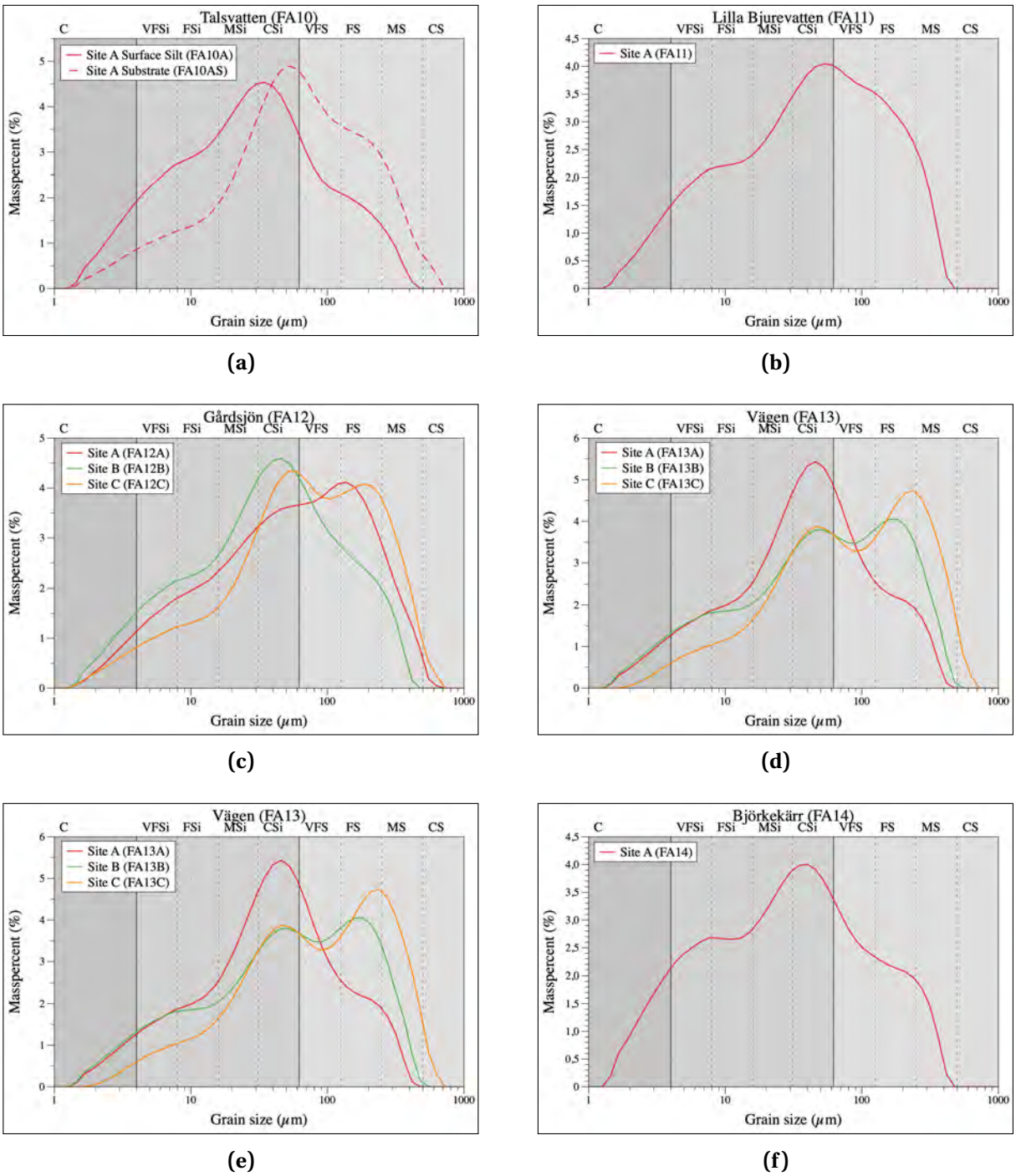

Figure A.2: Grain-size distributions

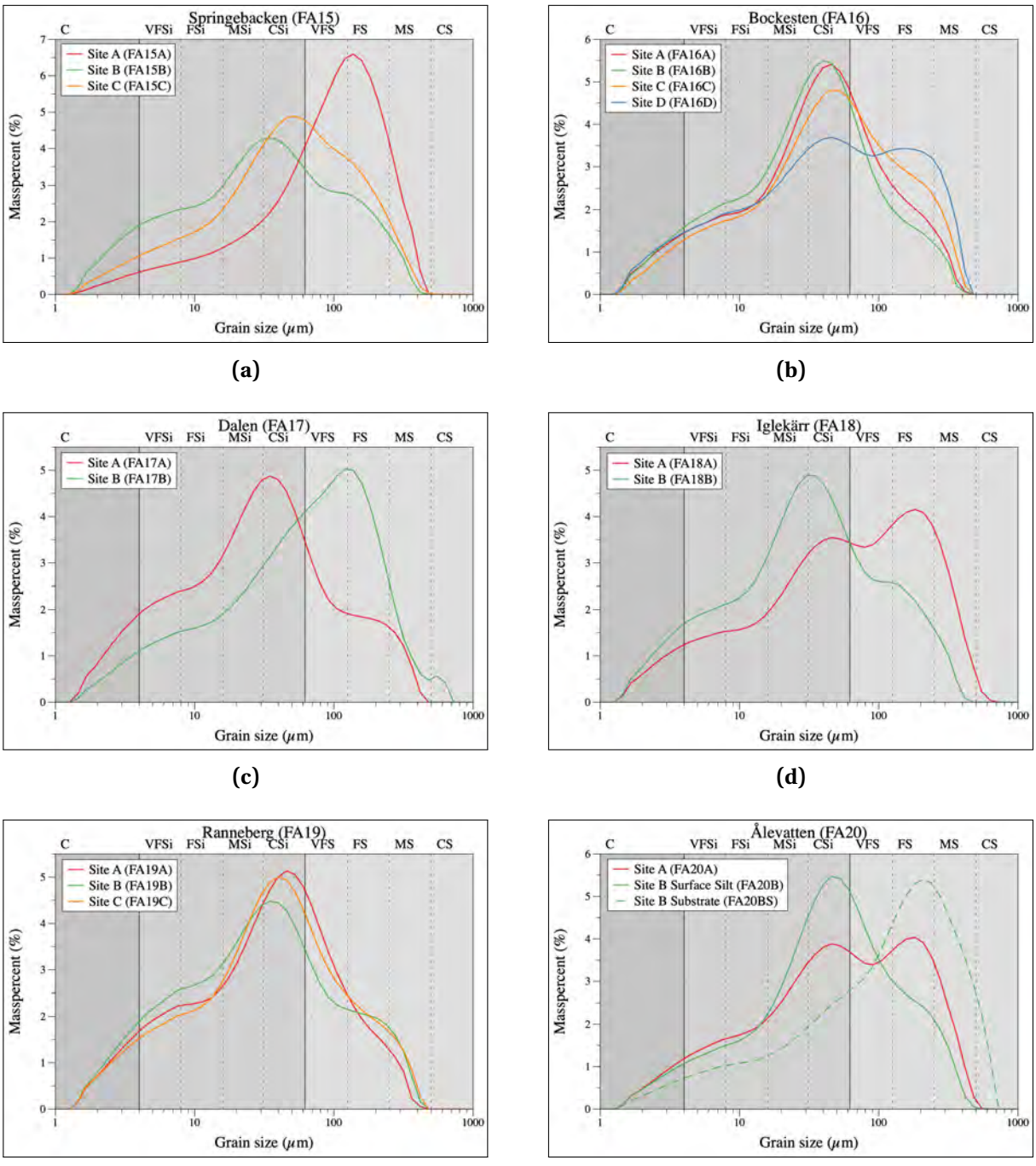

Figure A.3: Grain-size distributions

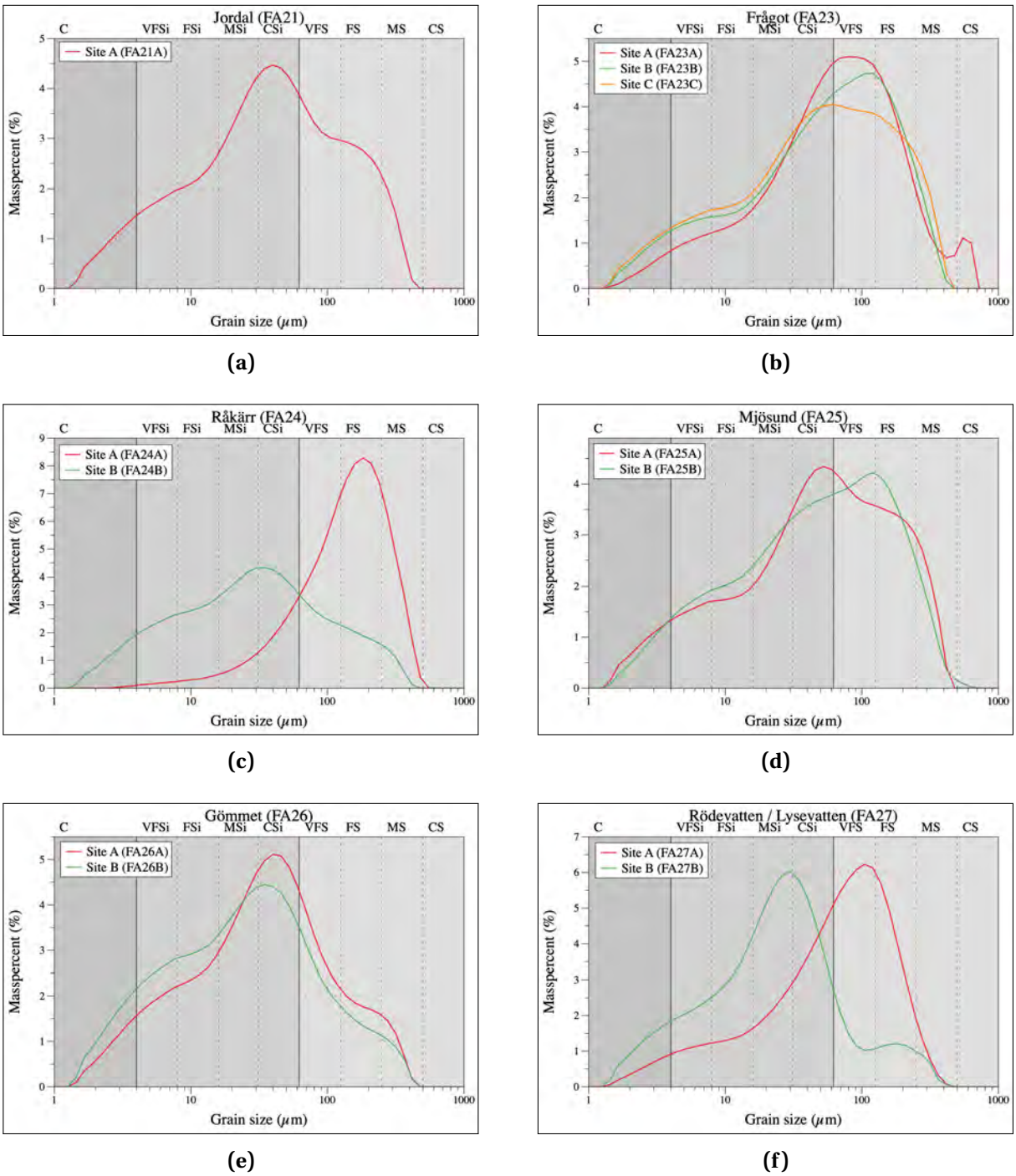

Figure A.4: Grain-size distributions

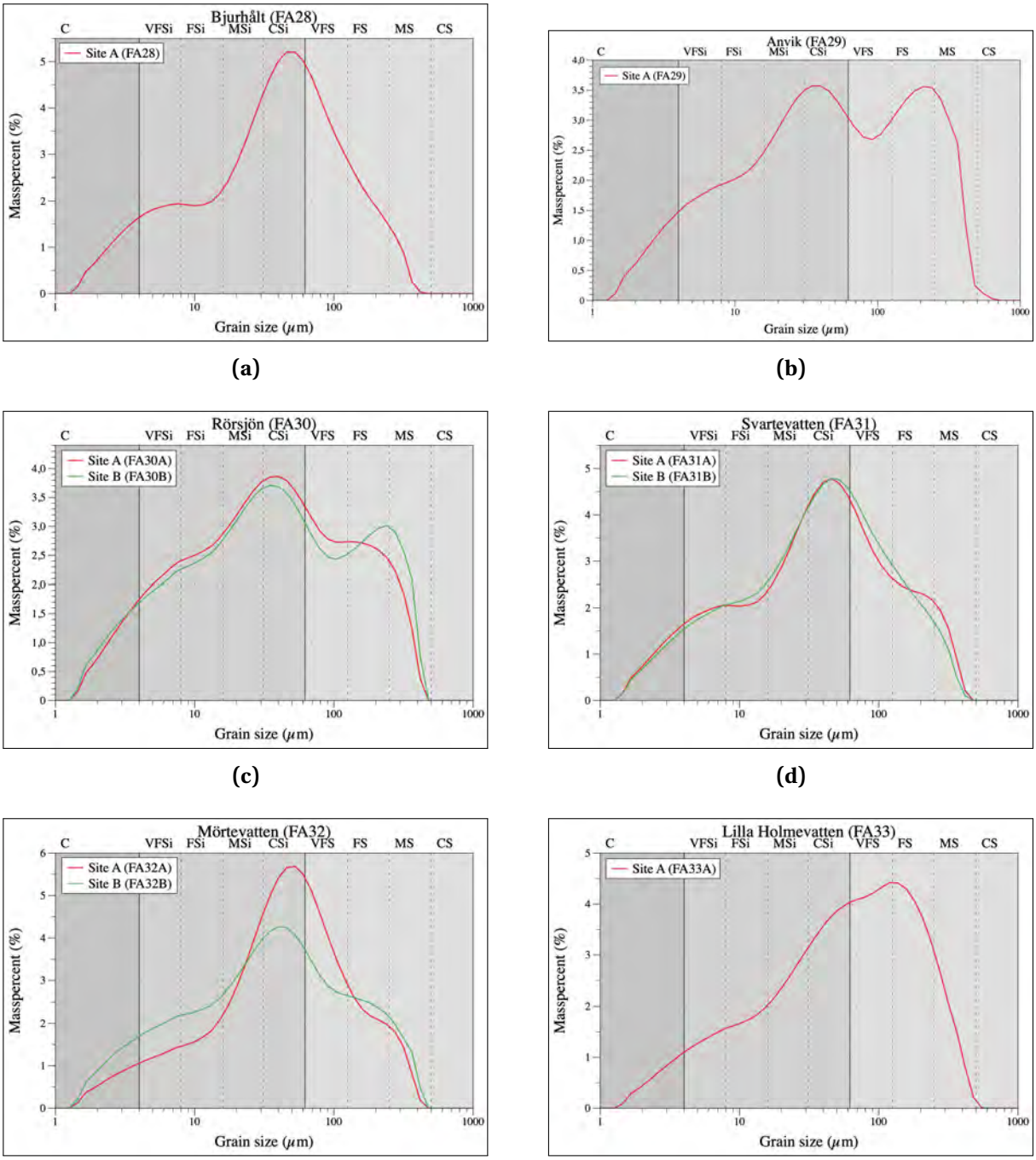

Figure A.5: Grain-size distributions

A.1.1 Appendix B

LUND UNIVERSITY

Lund Luminescence Laboratory
Department of Geology
Lund University

OSL dating report - Svartedalen

Submitters: Anna Hedeving & Fanny Ekström

Age summary

The quartz OSL ages of the five samples range in age from 1 ka to 7 ka (Table 1). All samples have nice, bright signals and relatively tight dose distributions.

Table 1. Summary of results (quartz data). CAM = Central Age Model. Preferred ages in bold. n = number of aliquots, w.c. = water content.

Lab no. Lund	Your no.	CAM age (ka)	Mean age (ka)	Dose (Gy)	n acc./total	Dose rate (Gy/ka)	w.c. (%)
20015	FA2AO	**5.0±0.3**	5.0±0.3	9.03±0.17	26/27	1.80±0.09	70
20142	FA2O1	**6.8±0.4**	6.9±0.4	14.73±0.44	30/30	2.13±0.11	63
20143	FA5BO	**6.8±0.5**	7.0±0.5	17.41±0.94	26/30	2.49±0.12	48
20144	FA18BO	**1.07±0.06**	1.08±0.06	1.86±0.03	30/33	1.72±0.08	74
20145	FA13BO	**4.3±0.2**	4.3±0.2	7.84±0.09	30/30	1.81±0.09	75

Lund, 2021-05-07

Helena Alexanderson
Lund Luminescence Laboratory

Sample preparation

Preparation included treatment with 10% HCl to remove carbonates, 10% H_2O_2 to remove any organic material and density separation at 2.62 g/cm^3 (LST Fastfloat). The quartz separate was then treated with 40% HF (30 min.; 20 min. for 20142) to remove remaining impurities and to etch the outer surface of the grains, and finally with 10% HCl to clean out any fluorides. Sieving was then done to extract the grain-size fractions selected for analysis.

Table 2. Sample information. Q=quartz.

Lab no. Lund	Site	Your no.	Altitude (m asl)	Depth (m)	Grain size (µm)	Mineral
20015	Svartedalen	FA2AO	135*	0.15*	63-90	Q
20142	Svartedalen	FA201	135	0.12	63-90	Q
20143	Svartedalen	FA5BO	138	0.25	63-90	Q
20144	Svartedalen	FA18BO	142	0.15	63-90	Q
20145	Svartedalen	FA13BO	155	0.15	63-90	Q

* These values are assumed based on information in an e-mail from the submitter where 20015 was stated to come from very close to 20142.

Dose rate and water content

The sediment dose rate was determined by high-resolution gamma spectrometry at the VKTA, Dresden, Germany and the total environmental dose rate was calculated in the DRAC online calculator (Durcan *et al.* 2015). The values of the environmental dose rate are in the range 1.7-2.5 Gy/ka (Table 1). These values are within the typical range for sandy deposits.

Table 3. Dose rate data.

Lab no. Lund	^{238}U (ppm)	^{232}Th (ppm)	^{40}K (%)
20015	2.5 ± 0.3	7.4 ± 0.5	1.67 ± 0.17
20142	2.5 ± 0.5	7.0 ± 0.6	2.13 ± 0.17
20143	4.3 ± 0.5	5.9 ± 0.4	2.05 ± 0.16
20144	2.6 ± 0.4	6.6 ± 0.5	1.64 ± 0.14
20145	4.1 ± 0.5	5.8 ± 0.4	1.52 ± 0.13

Water content

Water content was calculated after weighing sediment as it was taken out of the tube, after being saturated for 24 hours and after drying at 105°C for 24 hours (Table 4). For the calculation of the final age, the sediments from samples 20142 and 20145 are assumed to have had water content similar to the field water content since deposition and samples 20143-144 are assumed to have had water content similar to the field water content for 50% of the time and being completely dry for 50% of the time (based on information from the submitters). Sample 20015 was assumed to be similar to 20142. An uncertainty of 5% has been added to the selected water content for age calculation.
Age calculation with different water-content values can be done on request, if the hydrogeological circumstances suggest other conditions. Using higher water contents would lead to lower ages, and vice versa.

Table 4. Water content as measured in the samples.

Lab no. Lund	Field (weight%)	Saturated (weight%)	Selected (weight%)
20015	60	80	70
20142	63	77	63
20143	42	53	48
20144	54	94	74
20145	66	75	75

Dose

Measurement

Small (2-mm) single aliquots of 63-90 µm quartz (Fig. 1) were analysed in a Risø TL/OSL reader model DA-20 (Bøtter-Jensen *et al.* 2010). Single Aliquot Regeneration (SAR) protocols were used, with pre-heat and cutheat temperatures as in Table 5. OSL stimulation was by blue light sources (470 ± 30 nm) and detection was through 7.5 mm of U340 glass filter. The first 0.8 s of the signal were integrated for the peak, and the following 0.8 s for background. The laboratory dose rate was ~0.19 Gy/s.

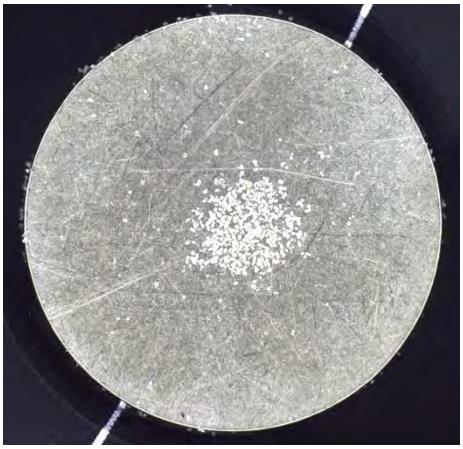

Fig. 1. Example of an aliquot from sample 20145. The disc is 9.8 mm in diameter and the grains are placed in a ~2-mm diameter cluster in the middle. Each aliquot consists of a few hundred 63-90 µm grains.

Luminescence characteristics

Tests have been carried out to adapt the analytical protocol (SAR-protocols) to suit each sample (Table 5). All samples have a strong and clear fast signal component, which is necessary for reliable dating (Fig. 2). The signals show a steady growth with dose (Fig. 3).

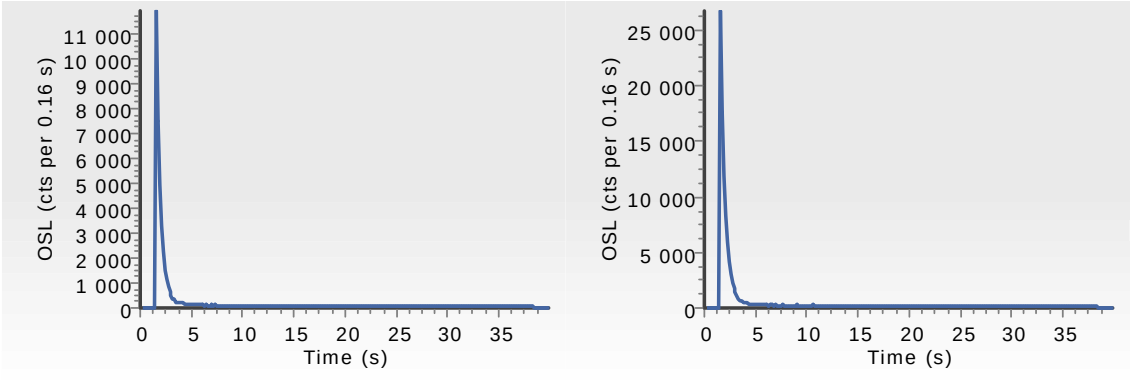

Fig. 2. Examples of OSL decay curves (left sample 20143, right 20144). The strong peak which rapidly decays to a low background shows the luminescence signal is dominated by a fast component. It can be noted that the sample with the lower dose (younger; 20144) appears brighter than the sample with the higher dose (20143).

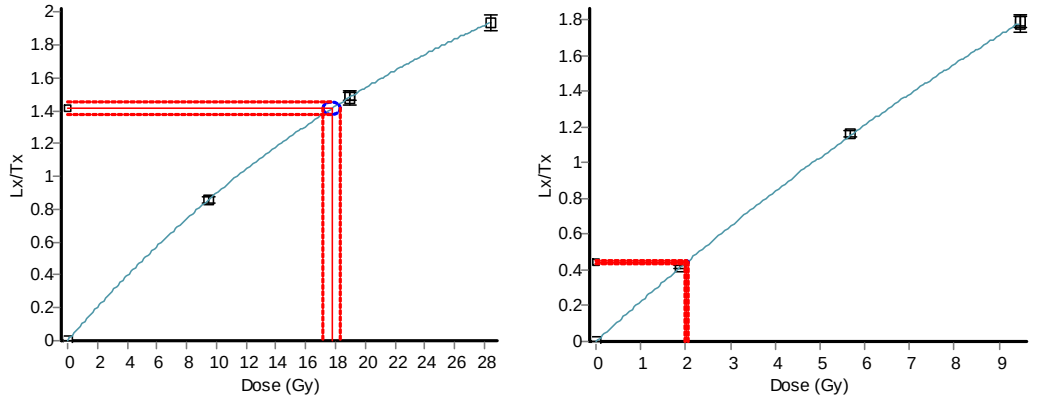

Fig. 3. Examples of OSL growth curves, showing a steady rise of signal with dose (left sample 20143, right 20144).

IR-test

The mean IR/blue ratios for all samples are given in Table 5. If the ratio was ≤10% for all tested aliquots for a certain sample, it was assumed to be pure quartz (insignificant feldspar contamination). If the ratio was >10% for a few of the aliquots, an extra recycling with post-infrared blue stimulation was added to the SAR-protocol, to identify any aliquots with significant feldspar contamination (Duller 2003). If all aliquots from a sample had ratios >10% the sample was analysed with post-IR blue stimulation and if the ratio was >>10%, pulsed stimulation was used. See Table 5 footnotes for references.

Table 5. Settings for SAR-protocols, dose recovery ratios and, for quartz separates, apparent feldspar contamination. For samples measured with IRB protocol, the IR/B ratio is the mean of all measured aliquots, for samples measured with B protocol, it is the mean of three aliquots measured with IRB stimulation.

Lab no. Lund	Grain size (µm)	Mean IR/B (%)	Stimulation	Preheat/ cutheat (°C)	Signal	Dose recovery ratio
20015	63-90	3	IRB	200/160	OSL	0.97±0.01
20142	63-90	1	B	180/160	OSL	0.89±0.03
20143	63-90	2	B	180/160	OSL	0.87±0.04
20144	63-90	1	B	180/160	OSL	0.99±0.01
20145	63-90	0	B	180/160	OSL	0.92±0.01

Explanation and references for analytical protocols used here.
B: blue stimulation (Murray & Wintle 2000, 2003)
IRB: post-infrared blue stimulation (Banerjee *et al.* 2001)

Dose recovery and preheat plateau tests

Preheat plateau tests and dose recovery (measuring a known given dose) with different preheat temperatures were used to determine which pre-heat and cutheat temperature combination was most suitable for the samples (Fig. 4, Fig. 5). The mean dose recovery ratio for the selected temperature settings for all samples reported here is for OSL 0.93±0.02 (n=15; OD= 3.1%). The ideal dose recovery ratio is 1.0 but values between 0.9 and 1.1 are generally accepted.

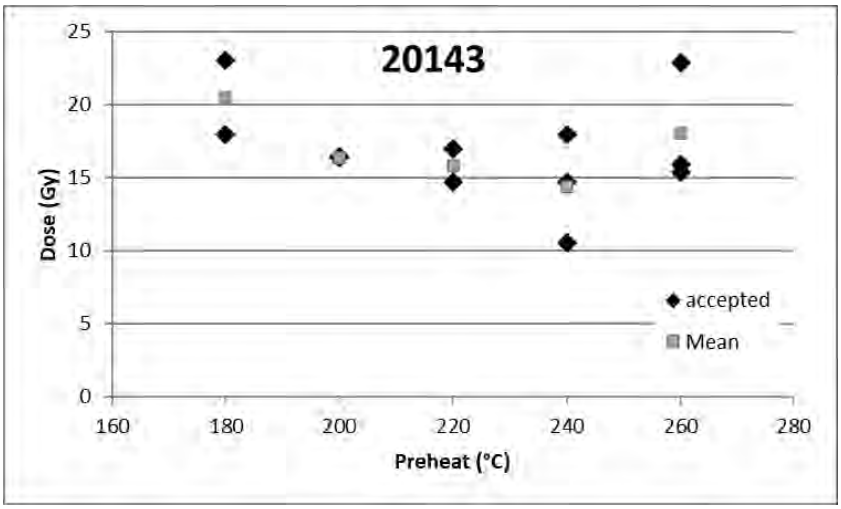

Fig. 4. The preheat plateau test for sample 20143 shows the dependence of dose on preheat and cutheat temperatures.

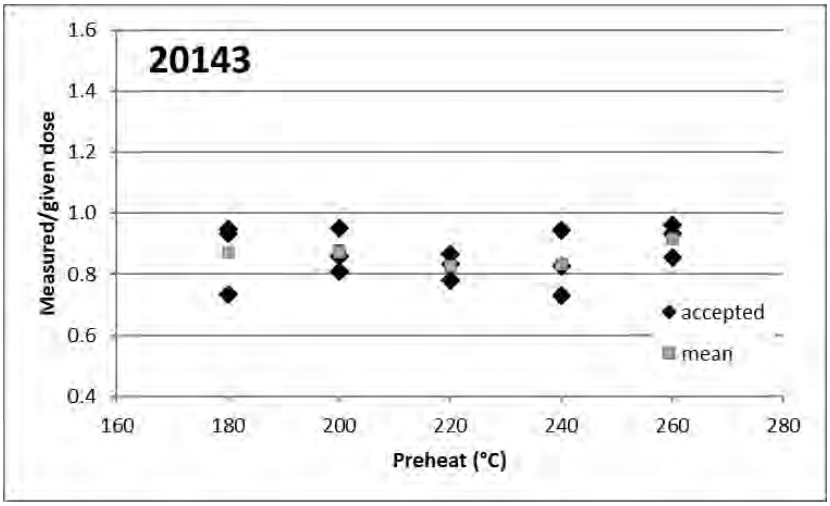

Fig. 5. Dose recoveries done with different preheat and cutheat temperatures for sample 20143.

Recycling and recuperation

The mean recycling ratio, which shows the ability to repeat a measurement, is 1.028±0.002 (n=142) for all quartz samples. The ideal value is 1.0, but values (including their uncertainties) between 0.9 and 1.1 are generally accepted. Recuperation, i.e. the response to zero dose, is on average 0.04% of the natural signal. Values <5% are generally accepted.

Dose calculation

Doses were calculated in the Risø Analyst 4.57 software with exponential curve fitting. Aliquots were accepted if they had a test dose error of <10%, a recycling ratio within 10% of unity and recuperation <5% of the natural signal. Very few of the measured aliquots had to be rejected, mainly due to failed

recycling ratios. A test with bleached but unheated quartz from sample 20143 showed that there is no thermal transfer effect that needs to be considered (measured dose 0.03±0.03 Gy).

Statistic treatment of dose distributions

Doses for age calculation were calculated using the arithmetic mean (Guérin *et al.* 2017) and the Central Age Model (CAM; Galbraith *et al.* 1999; Burow 2021).

Sample dose data

On the following pages, dose data and statistics for each sample are listed.
RSD = relative standard deviation, OD = overdispersion

Sample 20015

Table 6. Individual dose measurements sorted in order of size.

No.	Q-OSL dose (Gy)
1	7.1 ± 0.2
2	7.2 ± 0.2
3	7.3 ± 0.2
4	7.5 ± 0.2
5	8.2 ± 0.2
6	8.3 ± 0.2
7	9.0 ± 0.2
8	9.0 ± 0.2
9	9.0 ± 0.2
10	9.1 ± 0.2
11	9.1 ± 0.2
12	9.1 ± 0.2
13	9.3 ± 0.2
14	9.3 ± 0.3
15	9.4 ± 0.3
16	9.4 ± 0.2
17	9.5 ± 0.2
18	9.5 ± 0.3
19	9.6 ± 0.2
20	9.6 ± 0.3
21	9.6 ± 0.3
22	9.7 ± 0.3
23	9.8 ± 0.2
24	9.8 ± 0.3
25	10.0 ± 0.3
26	10.3 ± 0.3

Table 7. Equivalent dose (D_e) statistics for quartz.

Mean	9.0	Gy	
Median	9.3	Gy	
Standard error	0.2	Gy	
Standard deviation	0.9	Gy	
RSD	9.8		
Skewness	-1.11		not significant
Kurtosis	0.26		not significant
Minimum	7	Gy	
Maximum	10	Gy	
Number	26		
CAM	9.0	0.2	Gy
OD	9.3	1.5	%

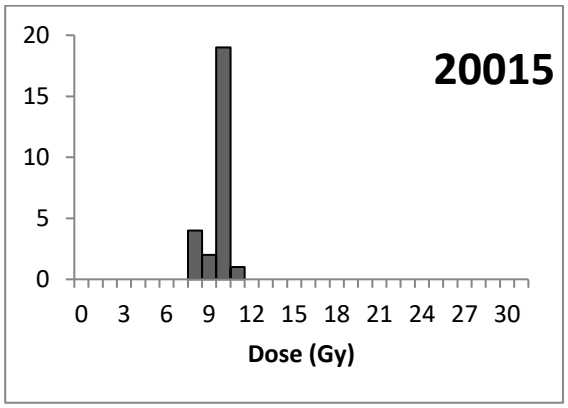

Fig. 6. Histogram of D_e values for quartz

Sample 20142

Table 8. Individual dose measurements sorted in order of size.

No.	Q-OSL dose (Gy)
1	8.4 ± 0.2
2	9.3 ± 0.3
3	11.8 ± 0.3
4	12.3 ± 0.4
5	12.4 ± 0.4
6	12.5 ± 0.4
7	13.1 ± 0.4
8	13.6 ± 0.4
9	13.7 ± 0.4
10	13.8 ± 0.4
11	13.8 ± 0.4
12	14.0 ± 0.4
13	14.6 ± 0.4
14	14.8 ± 0.4
15	15.1 ± 0.5
16	15.1 ± 0.5
17	15.3 ± 0.6
18	15.5 ± 0.5
19	15.8 ± 0.5
20	15.9 ± 0.5
21	16.0 ± 0.5
22	16.1 ± 0.5
23	16.1 ± 0.6
24	16.6 ± 0.5
25	16.7 ± 0.5
26	17.2 ± 0.5
27	17.9 ± 0.6
28	17.9 ± 0.6
29	18.3 ± 0.7
30	18.6 ± 0.6

Table 9. Equivalent dose (D_e) statistics for quartz.

Mean	14.7	Gy	
Median	15.1	Gy	
Standard error	0.4	Gy	
Standard deviation	2.4	Gy	
RSD	16.5		
Skewness	-0.71		not significant
Kurtosis	0.65		not significant
Minimum	8	Gy	
Maximum	19	Gy	
Number	30		
CAM	14.5	0.5	Gy
OD	17.4	2.4	%

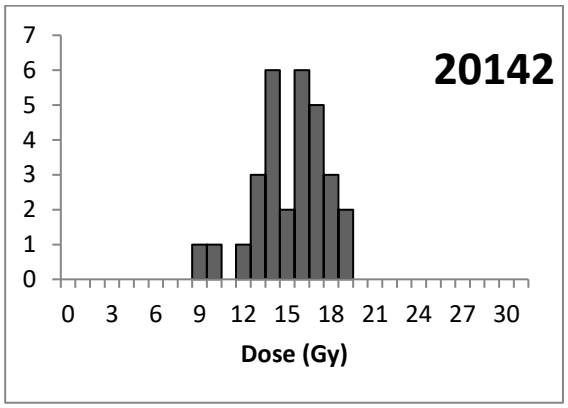

Fig. 7. Histogram of D_e values for quartz.

Sample 20143

Table 10. Individual dose measurements sorted in order of size.

No.	Q-OSL dose (Gy)
1	10.3 ± 0.4
2	11.1 ± 0.4
3	11.6 ± 0.6
4	13.4 ± 0.5
5	13.8 ± 0.5
6	14.4 ± 0.5
7	14.4 ± 0.6
8	14.6 ± 0.4
9	15.9 ± 0.6
10	16.1 ± 0.7
11	16.5 ± 0.8
12	16.8 ± 1.0
13	16.9 ± 0.7
14	17.8 ± 0.6
15	17.8 ± 1.1
16	17.9 ± 0.6
17	18.0 ± 0.9
18	18.0 ± 1.3
19	18.2 ± 0.8
20	18.5 ± 0.6
21	19.0 ± 1.2
22	20.0 ± 0.8
23	20.2 ± 1.0
24	23.0 ± 0.8
25	24.0 ± 0.9
26	34.5 ± 1.2

Table 11. Equivalent dose (D_e) statistics for quartz. Note, if the apparent outlier at 34 Gy is removed, the dose distribution is no longer significantly skewed. Keeping it does not however change the mean value significantly.

Mean	17.4	Gy	
Median	17.3	Gy	
Standard error	0.9	Gy	
Standard deviation	4.8	Gy	
RSD	27.5		
Skewness	1.77		significant
Kurtosis	5.74		significant
Minimum	10	Gy	
Maximum	34	Gy	
Number	26		
CAM	16.9	0.8	Gy
OD	24.2	3.5	%

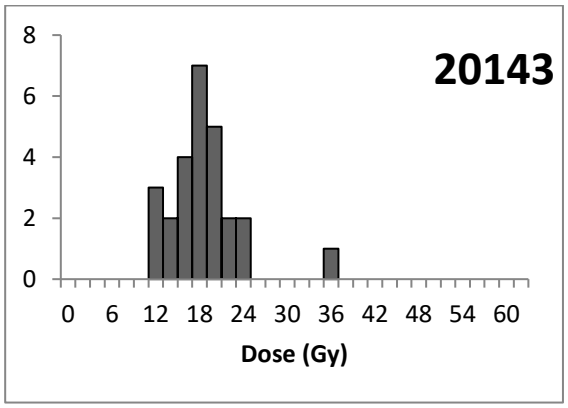

Fig. 8. Histogram of D_e values for quartz.

Sample 20144

Table 12. Individual dose measurements sorted in order of size.

No.	Q-OSL dose (Gy)
1	1.59 ± 0.04
2	1.63 ± 0.04
3	1.66 ± 0.05
4	1.68 ± 0.05
5	1.69 ± 0.05
6	1.70 ± 0.06
7	1.74 ± 0.04
8	1.78 ± 0.06
9	1.78 ± 0.04
10	1.78 ± 0.05
11	1.79 ± 0.06
12	1.80 ± 0.05
13	1.80 ± 0.04
14	1.81 ± 0.05
15	1.84 ± 0.07
16	1.88 ± 0.05
17	1.88 ± 0.05
18	1.90 ± 0.10
19	1.94 ± 0.09
20	1.96 ± 0.05
21	1.97 ± 0.10
22	1.97 ± 0.09
23	1.98 ± 0.08
24	1.99 ± 0.06
25	2.01 ± 0.11
26	2.02 ± 0.05
27	2.04 ± 0.07
28	2.04 ± 0.17
29	2.07 ± 0.13
30	2.14 ± 0.08

Table 13. Equivalent dose (D_e) statistics for quartz.

Mean	1.86	Gy	
Median	1.86	Gy	
Standard error	0.03	Gy	
Standard deviation	0.15	Gy	
RSD	7.8		
Skewness	-0.06		not significant
Kurtosis	-0.94		not significant
Minimum	1.6	Gy	
Maximum	2.1	Gy	
Number	30		
CAM	1.84	0.03	Gy
OD	6.2	1.2	%

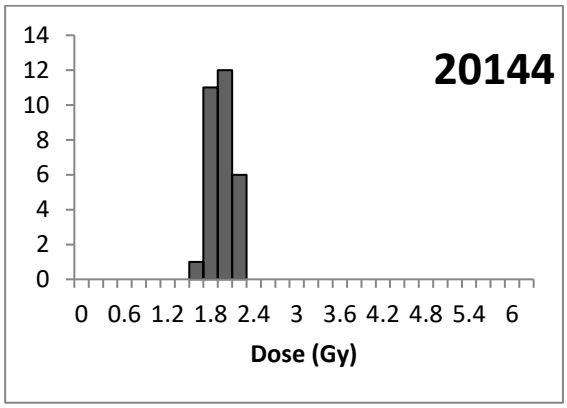

Fig. 9. Histogram of D_e values for quartz.

Sample 20145

Table 14. Individual dose measurements sorted in order of size.

No.	Q-OSL dose (Gy)
1	6.9 ± 0.2
2	7.0 ± 0.2
3	7.1 ± 0.2
4	7.2 ± 0.2
5	7.3 ± 0.2
6	7.3 ± 0.2
7	7.4 ± 0.2
8	7.5 ± 0.3
9	7.5 ± 0.2
10	7.6 ± 0.2
11	7.6 ± 0.2
12	7.7 ± 0.2
13	7.7 ± 0.2
14	7.8 ± 0.2
15	7.8 ± 0.2
16	8.0 ± 0.2
17	8.0 ± 0.2
18	8.0 ± 0.2
19	8.0 ± 0.2
20	8.1 ± 0.2
21	8.1 ± 0.2
22	8.1 ± 0.2
23	8.2 ± 0.2
24	8.2 ± 0.2
25	8.2 ± 0.2
26	8.3 ± 0.2
27	8.4 ± 0.2
28	8.5 ± 0.2
29	8.8 ± 0.3
30	8.9 ± 0.2

Table 15. Equivalent dose (D_e) statistics for quartz.

Mean	7.8	Gy	
Median	7.9	Gy	
Standard error	0.1	Gy	
Standard deviation	0.5	Gy	
RSD	6.4		
Skewness	-0.02		not significant
Kurtosis	-0.47		not significant
Minimum	7	Gy	
Maximum	9	Gy	
Number	30		
CAM	7.8	0.1	Gy
OD	4.8	1.1	%

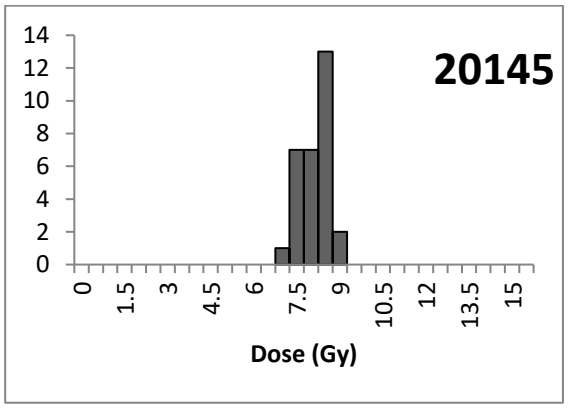

Fig. 10. Histogram of D_e values for quartz.

References

Banerjee, D., Murray, A. S., Bøtter-Jensen, L. & Lang, A. 2001: Equivalent dose estimation using a single aliquot of polymineral fine grains. *Radiation Measurements 33*, 73-94.

Burow, C. 2021: calc_CentralDose(): Apply the central age model (CAM) after Galbraith et al. (1999) to a given De distribution. Function version 1.4.0. *In* Kreutzer, S., Burow, C., Dietze, M., Fuchs, M. C., Schmidt, C., Fischer, M. & Friedrich, J. (eds.): *Luminescence: Comprehensive Luminescence Dating Data AnalysisR package version 0.9.7.* Function version 1.3.2. ed., https://CRAN.R-project.org/package=Luminescence.

Bøtter-Jensen, L., Thomsen, K. J. & Jain, M. 2010: Review of optically stimulated luminescence (OSL) instrumental developments for retrospective dosimetry. *Radiation Measurements 45*, 253-257.

Duller, G. A. T. 2003: Distinguishing quartz and feldspar in single grain luminescence measurements. *Radiation Measurements 37*, 161-165.

Durcan, J. A., King, G. E. & Duller, G. A. T. 2015: DRAC: Dose Rate and Age Calculator for trapped charge dating. *Quaternary Geochronology 28*, 54-61.

Galbraith, R. F., Roberts, R. G., Laslett, G. M., Yoshida, H. & Olley, J. M. 1999: Optical dating of single and multiple grains of quartz from Jinmium rock shelter, northern Australia. Part I: experimental design and statistical models. *Archaeometry 41*, 339-364.

Guérin, G., Christophe, C., Philippe, A., Murray, A. S., Thomsen, K. J., Tribolo, C., Urbanova, P., Jain, M., Guibert, P., Mercier, N., Kreutzer, S. & Lahaye, C. 2017: Absorbed dose, equivalent dose, measured dose rates, and implications for OSL age estimates: Introducing the Average Dose Model. *Quaternary Geochronology 41*, 163-173.

Murray, A. S. & Wintle, A. G. 2000: Luminescence dating of quartz using an improved single-aliquot regenerative-dose protocol. *Radiation Measurements 32*, 57-73.

Murray, A. S. & Wintle, A. G. 2003: The single aliquot regenerative dose protocol: potential for improvements in reliability. *Radiation Measurements 37*, 377-381.

The work leading up to the results presented in this report has been carried out by:

Roos van Wees and Ingrid Bejarano Arias, master students/laboratory assistants, Lund Luminescence Laboratory (sample preparation 20015)

Helena Alexanderson, professor, Lund Luminescence Laboratory (sample preparation, measurement, analysis, compilation)